World Electric Vehicle Journal

MDPI

Article

An Economic Velocity Planning Strategy Based on Driving Style and Improved Dynamic Programming for a Hybrid Electric Truck

Yuting Li, Rong Yang *, Zhengteng Wu, Wei Huang and Minmin Xu

College of Mechanical Engineering, Guangxi University, Nanning 530004, China; liyuting0813@163.com (Y.L.); wuzhengteng0725@163.com (Z.W.); buaahw@126.com (W.H.); mmxu@gxu.edu.cn (M.X.)
* Correspondence: yangrong0907@163.com

Abstract: The power coupling equation and energy consumption model for enhancing the fuel economy and power performance of plug-in hybrid electric trucks (PHETs) are proposed based on the economic velocity planning strategy (EVPS-DSIDP), which takes into account the driving style and an improved dynamic programming (IDP) algorithm. This strategy employs a fuzzy controller to identify the driving style, and optimizes the efficiency and accuracy of the conventional dynamic programming (DP) algorithm by associating decision variables, dynamically adjusting the discretization step size, and restricting the state space. Additionally, a penalty function is introduced to enhance the robustness of the DP algorithm. Under our EVPS-DSIDP, the variation of velocity is liberated from the constraints of fixed driving conditions, and directly correlates with road information and driving styles, which is of significant importance for addressing energy management issues in real-time traffic conditions. Moreover, the proposed IDP algorithm can improve computational efficiency while ensuring calculation accuracy, thereby greatly enhancing the potential for the practical application of this algorithm in real-world vehicle scenarios. The simulation results demonstrate that compared to the rule-based control strategy, the application of the proposed EVPS-DSIDP in the economy velocity planning strategy can achieve an average reduction of 2.88% in economic costs and 10.6% in travel time across different driving styles. This approach offers a more comprehensive optimization of both fuel economy and power performance.

Keywords: energy management strategy; plug-in hybrid electric truck; economic velocity planning; driving style; fuzzy controller; dynamic programming

Citation: Li, Y.; Yang, R.; Wu, Z.; Huang, W.; Xu, M. An Economic Velocity Planning Strategy Based on Driving Style and Improved Dynamic Programming for a Hybrid Electric Truck. *World Electr. Veh. J.* **2023**, *14*, 194. https://doi.org/10.3390/wevj14070194

Academic Editor: Ghanim A. Putrus

Received: 9 June 2023
Revised: 14 July 2023
Accepted: 19 July 2023
Published: 21 July 2023

1. Introduction

Traditional internal combustion engine trucks use fossil fuels, and their emissions of carbon dioxide and other harmful substances have a growing impact on the environment, making it difficult to comply with increasingly stringent fuel consumption and emission regulations. Therefore, hybrid and pure electric technologies have been rapidly developed. Although pure electric trucks have many advantages compared to traditional trucks, such as low emissions, low noise, and low operating costs, they also have some limitations, including limited range, inadequate charging infrastructure, long charging times, and a relatively lower payload capacity. Therefore, plug-in hybrid technology is considered to have broad prospects in the trucking industry [1].

Plug-in hybrid electric trucks (PHETs) can enjoy the advantages of pure electric vehicles while fully utilizing the stable power output provided by the internal combustion engine, thus achieving a balance between fuel economy and power performance. But its energy management strategy (EMS) directly influences their fuel economy, power performance, and emission [2]. In order to save energy and reduce emissions, the selection of effective algorithms for controlling hybrid electric vehicles has become a research focus [3,4]. Common EMSs include rule-based (RB) energy management strategy [5–7], equivalent

fuel consumption minimization strategy (ECMS) [8–10], Pontryagin's minimum principle (PMP) [11–13], model predictive control strategy (MPC) [14–16], etc. However, these strategies are mostly applied under fixed driving conditions, limiting the optimization of vehicle performance. In real-world situations, the driving conditions of vehicles are not fixed. In order to better optimize vehicle performance, research on optimization algorithms for variable driving conditions has gradually emerged [17,18]. The dynamic programming (DP) algorithm offers advantages such as finding the optimal solution, considering long-term consequences, and being easy to understand and implement [19]. Therefore, this study focuses on the research of economic velocity planning strategies with the DP algorithm as the core.

The core parameters of the DP algorithm are decision variables and state variables. The former represents all possible actions that can be taken at each stage, while the latter represents the state of the system when these actions are executed. Both decision variables and state variables need to be discretized on a grid [20]. The treatment of the grid in this process is crucial, as it should avoid uncontrolled computational expansion, known as the "curse of dimensionality" [21], while ensuring high accuracy during computation.

Currently, measures can be taken to optimize the DP algorithm, significantly reducing computation time without compromising the overall optimization performance. In reference [22], two different methods were employed to optimize the computation grid: the first method reduces the evaluation grid of the system model by using redundant control points, while the second method reconstructs the system model to minimize redundant control and system feasibility grids before conducting multidimensional interpolation. Although this approach has proven effective for DP algorithms that involve redundant control, its effectiveness has not been demonstrated for other DP algorithms that deal with non-redundant control. Reference [23] introduces a new variable step-size grid approach for optimizing the application of DP in economic velocity planning. It overcomes interpolation errors caused by discretization by adjusting different discrete step sizes and improves computational efficiency. Compared to a fixed step-size configuration, this method significantly reduces computation time while sacrificing only a small degree of accuracy. Although this method considers "horizontal (step size)" optimization of the grid, it does not simultaneously consider "vertical (velocity)" optimization of the grid, leaving room for further improvement. In reference [24], a two-step iterative DP algorithm was applied to optimize the vehicle's economic cruising velocity. In the first iteration, the range of state and control variables was reduced to alleviate computational and storage burdens, while in the second iteration, grid density was decreased to enhance optimization performance. Although this method demonstrated good results for optimizing cruising velocity in electric vehicles, its applicability to more complex PHET structures and non-cruising velocity planning scenarios has not been established.

Additionally, with the development of high-precision maps and vehicle-to-everything (V2X) communication [25], optimizing the velocity of vehicles through economic velocity planning—where vehicles follow a planned velocity—can effectively improve their fuel economy. Reference [26] developed eco-driving rules by optimizing economic velocity and gear selection to reduce fuel consumption under various congestion conditions on the same route. Reference [27] proposed a PMP algorithm based on traffic flow velocity, road speed limits, and road gradients, which provides economic velocity planning for vehicles to enhance overall fuel economy. Reference [28] developed an Eco-MS-Q algorithm that utilizes road information collected through vehicle-to-infrastructure (V2I) communication to predict and estimate the optimal velocity trajectory, optimizing fuel consumption when passing through multiple signalized intersections. Reference [29] designed an economic velocity planning strategy based on the principle of optimizing fuel economy during vehicle starts, stops, acceleration, and deceleration, while maintaining smooth velocity and a certain distance. Reference [30] explored the economic velocity planning of a P2 plug-in hybrid electric car, based on the predictable road information of the bend ahead, in order to achieve better energy economy while ensuring driving safety. Reference [31] proposed an

economic velocity planning strategy-based EMS within the MPC principle, considering the adaptive reference state of charge driving pattern. Reference [32] presented a real-time hierarchical effective and efficient co-optimization control strategy designed to plan economic velocity and achieve energy management in urban driving scenarios. Reference [33] proposed a reinforced equivalent consumption minimization strategy based on kinetic energy management and ECMS, which is applied to economic velocity planning. The research findings of these scholars indicate that economic velocity planning can effectively reduce vehicle energy consumption. However, the aforementioned studies on economic velocity planning primarily focus on pure electric vehicles and conventional fuel vehicles, with limited research on economic velocity planning for hybrid electric vehicles and minimal consideration of the driver's driving style in economic velocity planning.

In general, within the existing research on economic velocity planning strategies, numerous scholars have conducted extensive investigations using different optimization control methods for powertrain systems of either pure electric vehicles or conventional fuel vehicles, resulting in significant achievements. However, most control strategies focus only on specific environments or consider only single/partial operating conditions, thereby lacking generality. Furthermore, the influence of driver behavior on velocity planning is often overlooked in the majority of economic velocity planning studies. The fuel economy and power performance of a vehicle are interrelated and mutually influenced, and failing to control them appropriately can easily lead to a substantial increase in travel time while attempting to reduce economic costs, ultimately resulting in suboptimal outcomes.

The innovative aspects and contributions of this article can be summarized as follows:

- Simplifying vehicle gear shifting and operating mode selection logic by associating them with velocity.
- Implementing driving style recognition using a fuzzy controller.
- Introducing an IDP algorithm to achieve better computational efficiency and accuracy.
- Developing the EVPS-DSIDP based on the driving style and the IDP algorithm.
- Demonstrating improved fuel economy and power performance with the EVPS-DSIDP under different driving styles.

This study aims to achieve rational economic velocity planning by employing an adaptive control strategy that combines driving style and improved dynamic programming (IDP), under the condition of sufficient battery state of charge (SOC). The remainder of this study is organized as follows: Section 2 establishes a vehicle energy consumption model for the PHET based on experimental data. Section 3 presents the economic velocity planning strategy for the PHET by integrating driving style and the IDP algorithm. Section 4 validates the proposed economic velocity planning strategy through simulation tests. Finally, Section 5 provides conclusions.

2. Modeling of Hybrid Power System Based on Dual Planetary Gear

2.1. Overall Structure

The subject of this study is a dual planetary power-split PHET, as shown in Figure 1. The vehicle's powertrain system comprises three power sources: two electric motors (MG1, MG2) and an engine. The front-row planetary gear (PG1) serves as the power-split mechanism, where the sun gear (S1) of PG1 is connected to the motor MG1. The carrier (C1) of PG1 is connected to the engine through a buffer locking mechanism (BLM). The buffer section of BLM mitigates impacts and vibrations through energy absorption, while the locking section fixes C1 using locking and clamping mechanisms, thereby altering the power-split mode of PG1. The ring gear (R1) of PG1 is connected to the carrier (C2) of rear-row planetary gear (PG2), enabling power output to the gearbox. The sun gear (S2) of PG2 is connected to the motor MG2, and the ring gear (R2) of PG2 is fixed to the housing, creating an equivalent fixed gear ratio gear transmission mechanism. This configuration not only decouples the engine torque and speed from the vehicle's physical state, but also enables smooth transition between different operating modes, fully exploiting the optimal performance of the entire powertrain system.

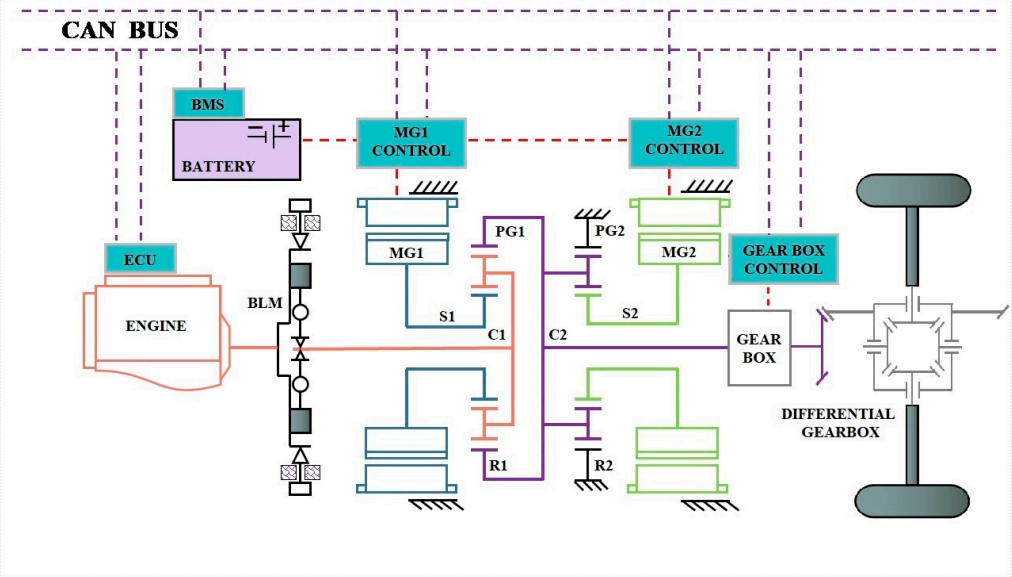

Figure 1. Configuration of the PHET.

The PHET studied in this study is applied in heavy-duty commercial vehicles used in industries such as freight transport. The proper selection of components is crucial to ensure its optimal performance in terms of fuel economy and power. The main parameters of each component of the PHET are listed in Table 1.

Table 1. Parameters of PHET.

Symbol	Component	Parameter (Unit)	Value
m	Vehicle	Vehicle curb mass (kg)	31,000
R_{wh}		Tire rolling radius (m)	0.528
A		Frontal area (m^2)	7.5
C_D		Wind resistance coefficient	0.56
f_r		Rolling resistance coefficient	0.015
δ		Rotational mass conversion coefficient	1.1
P_{Eng}^{Max}	Engine	Maximum power (kW)	240
T_{Eng}^{Max}		Maximum torque (N·m)	1400
n_{Eng}^{Max}		Maximum speed (rpm)	2200
ρ_{fuel}		Fuel density(kg/L)	0.76
P_{MG1}^{Max}	Motor	Maximum power (kW)	106
T_{MG1}^{Max}		Maximum torque (N·m)	340
n_{MG1}^{Max}		Maximum speed (rpm)	7500
P_{MG2}^{Max}		Maximum power (kW)	196
T_{MG2}^{Max}		Maximum torque (N·m)	375
n_{MG2}^{Max}		Maximum speed (rpm)	15,000
$k_{1,2}$	Transmission	PG1/PG2 characteristic parameter	4.4/5.7
i_g		Ratio of gear position	[6.3 2.1 1 0.86]
i_{fd}		Ratio of main reducer	5.1
C_{ele}	Economic cost	Electricity cost (RMB/kWh)	1
C_{fuel}		Fuel cost (RMB/L)	7.5

2.2. Model for the Key Components

The model construction and algorithm optimization in this study were carried out in MATLAB. The models of key components are ideal models, neglecting factors such as shifting time, frictional losses between components, and energy losses due to engine and motor start-stop operations during simulation.

2.2.1. Engine Model

One of the key focuses of this study is to optimize the fuel economy during vehicle operation, which essentially involves optimizing the operating points of the engine and motors. In this study, the effective brake-specific fuel consumption (BSFC) of the engine is obtained using chassis dynamometer experimental data. The BSFC is determined by the engine torque (T_{Eng}) and engine speed (n_{Eng}), as shown in Figure 2.

$$BSFC = f_{BSFC}(T_{Eng}, n_{Eng}) \tag{1}$$

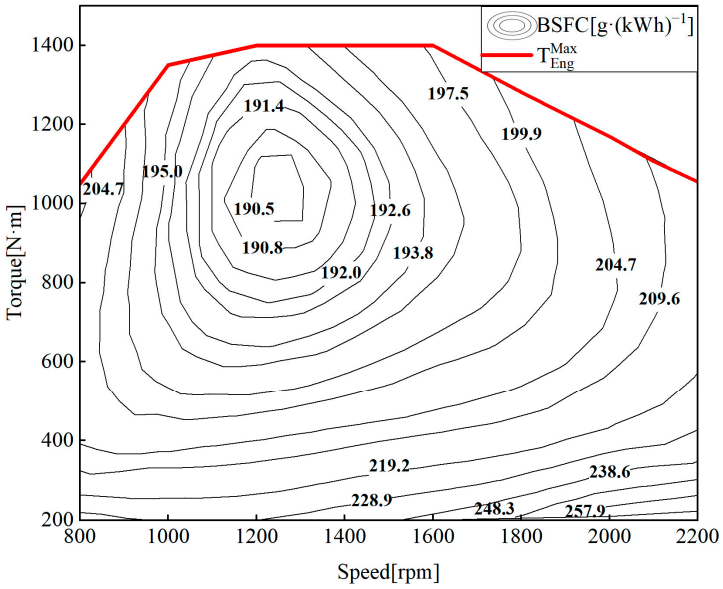

Figure 2. Contour map of engine fuel consumption and full load characteristics.

The fuel consumption per unit time of the engine can be expressed as:

$$\dot{V}_{fuel}^{Eng} = \frac{T_{Eng} \times n_{Eng} \times BSFC}{9550 \times 3.6 \times 10^6 \times \rho_{fuel}} \tag{2}$$

2.2.2. Electric Motor Model

This study involves two motors, each with different operating conditions and purposes, necessitating the use of motors with different specifications. MG2 is primarily utilized for driving and regenerative braking, while MG1 is mainly employed for torque compensation and controlling the engine operating point. The relationship between motor speed, torque, and efficiency is obtained through dynamometer test data for both motors. The efficiency maps for MG1 and MG2 are presented in Figures 3 and 4, respectively. Both motors can function as electric motors for propulsion as well as generators for power generation. The relationship between motor power, torque, speed, and efficiency can be expressed as:

$$\eta_{MG} = f_{eff}(T_{MG}, n_{MG}) \tag{3}$$

$$P_{MG\_E} = \underbrace{\frac{T_{MG} \cdot n_{MG}}{9550}}_{P_{MG}} \cdot \eta_{MG}^{-\mathrm{sgn}(P_{MG})} \tag{4}$$

where P_{MG_E} is the motor electric power, P_{MG} is the motor mechanical power, T_{MG} is the motor torque, and n_{MG} is the motor speed. When $P_{MG} > 0$, η_{MG} represents motor efficiency, and when $P_{MG} < 0$, it represents generator efficiency. $\mathrm{sgn}(x)$ is the sign function, and when $\mathrm{sgn}(x) = 1$, $x \geq 0$ is the motoring state; when $\mathrm{sgn}(x) = -1$, $x < 0$ is the generating state.

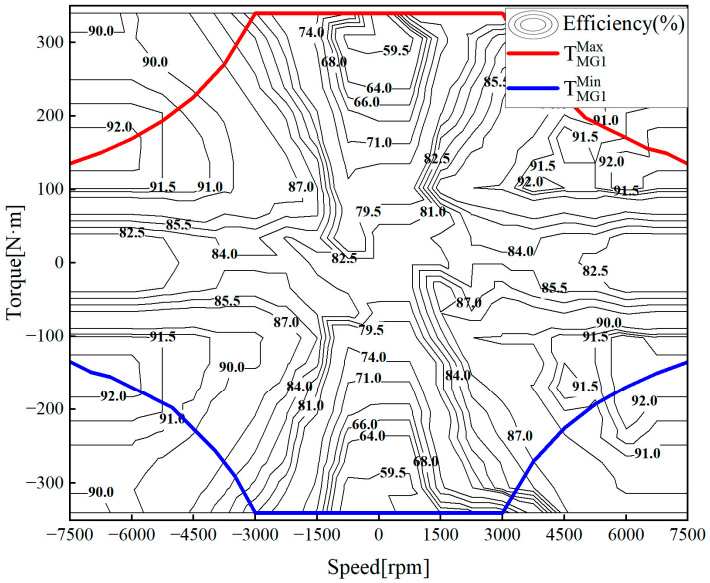

Figure 3. Efficiency map of MG1.

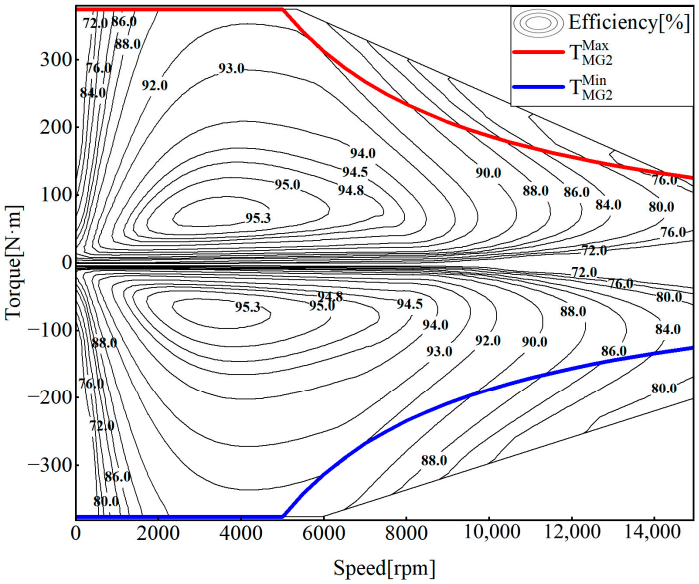

Figure 4. Efficiency map of MG2.

The electrical power consumed/generated by the two motors during operation can be expressed as:

$$P_{batt} = P_{MG1\_E} + P_{MG2\_E} \tag{5}$$

2.2.3. Planetary Gear Model

In the transmission system of the PHET, power transmission is determined by the speed and torque characteristics of dual planetary gears. The structure of the planetary gear, including the ring gear, planetary carrier, and sun gear, is illustrated in Figure 5, with their interconnections formed by the planetary gears.

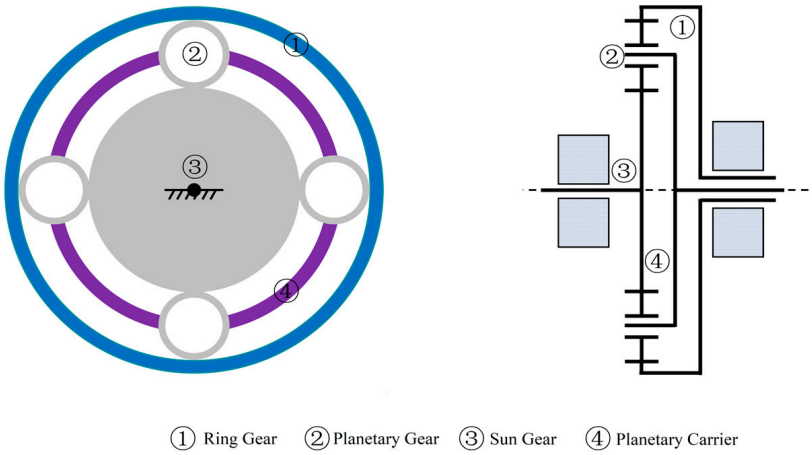

Figure 5. The structure of the planetary gear.

On the PG1, n_{S1}, n_{C1}, and n_{R1} represent the speeds of S1, C1, and R1, respectively, while k_{p1} is the characteristic parameter of the PG1. Similar symbol definitions apply to the PG2 $(n_{S2}, n_{C2}, n_{R2}$ and $k_{p2})$, with the difference being that R2 is fixed to the housing $(n_{R2} = 0)$. According to the speed balance equation between the components of the planetary gears, it can be determined that:

$$n_{S1} + k_{p1} n_{R1} - (1 + k_{p1}) n_{C1} = 0 \tag{6}$$

$$n_{S2} - (1 + k_{p2}) \cdot n_{C2} = 0 \tag{7}$$

Neglecting the inertia torques of the components, as well as the transmission efficiency losses and friction losses between gears, the power balance and torque equilibrium relationship of the PG1 can be derived. It can be expressed as:

$$\begin{cases} T_{S1} + T_{C1} + T_{R1} = 0 \\ n_{S1} T_{S1} + n_{C1} T_{C1} + n_{R1} T_{R1} = 0 \\ \frac{T_{S1}}{1} = \frac{T_{R1}}{k_{p1}} = -\frac{T_{C1}}{1 + k_{p1}} \end{cases} \tag{8}$$

where T_{S1}, T_{C1}, and T_{R1} are the torque on the sun gear, planetary carrier and gear ring of PG1, respectively. The similar formula applies to PG2 $(T_{S2}, T_{C2}$ and $T_{R2})$.

When the BLM is released, the external torque acting on C1 is provided by the engine.

$$T_{C1} = T_{Eng} \tag{9}$$

According to the relationship between the dual planetary gears, it can be determined that:

$$\begin{cases} n_{MG1} = n_{S1}, n_{MG2} = n_{S2}, n_{Eng} = n_{C1} \\ n_{out} = n_{C2}, n_{R2} = 0, n_{R1} = n_{C2} \\ T_{S1} = T_{MG1} \\ T_{S2} = T_{MG2} \\ T_{out} + T_{R1} + T_{C2} = 0 \end{cases} \tag{10}$$

where T_{out} is the output torque of the powertrain system.

2.3. Model for the Longitudinal Dynamics of Vehicle

According to the automotive theory, a mathematical model for the longitudinal dynamics of the PHET is established, and the T_{out} can be expressed as:

$$T_{out} = R_{wh}/i_{fd}/i_g \cdot [\underbrace{mgf_r \cos\alpha}_{F_{rolling}} + \underbrace{1/2C_D\rho_{air}Av^2}_{F_{air}} + \underbrace{\delta m dv/dt}_{F_{inertia}} + \underbrace{mg\sin\alpha}_{F_{gradiet}}] \quad (11)$$

where $F_{rolling}$ is the rolling resistance, F_{air} is the air resistance, $F_{inertia}$ is the acceleration resistance, and $F_{gradiet}$ is the ramp resistance. f_r is the rolling resistance coefficient, C_D is the wind resistance coefficient, ρ_{air} is the air density, A is the frontal area, and v is the vehicle velocity. α is the road ramp angle, and δ is the rotation mass conversion coefficient. R_{wh} is the tire rolling radius, i_{fd} is the transmission ratio of the main reducer, and i_g is the transmission ratio of gear position.

3. Economic Velocity Planning Strategy

3.1. Driving Style Recognition Based on Fuzzy Controller

One of the research focuses of this study is to integrate the driver's driving style into the economic velocity planning. In situations where braking is not required, drivers generally reflect their driving style through variations in the accelerator pedal (AP). Based on the longitudinal dynamics model of the vehicle, the energy consumption of the PHET during flat road driving is mainly concentrated during acceleration and steady-state driving. Since the velocity fluctuation is minimal during steady-state driving, this study primarily investigates the economic velocity planning of the vehicle under acceleration tendencies.

During driving, the driver's driving style is typically reflected through the variations in the AP and the change in AP between adjacent sampling points (dAP). Therefore, in this study, AP and dAP are introduced as input parameters for the driver model, and a fuzzy controller is employed for the driving style recognition. The fuzzy controller takes AP and dAP as input variables and outputs a power coefficient (γ). AP, dAP, and γ are divided into five fuzzy subsets:$\{NM, NS, ZO, PS, PM\}$. The definition range of AP and γ is [0, 1], and the definition range of dAP is $[-1, 1]$. The membership functions for inputs are shown in Figure 6. Correspondingly, the fuzzy rules are presented in Table 2, and the output surface of the fuzzy inference system is shown in Figure 7.

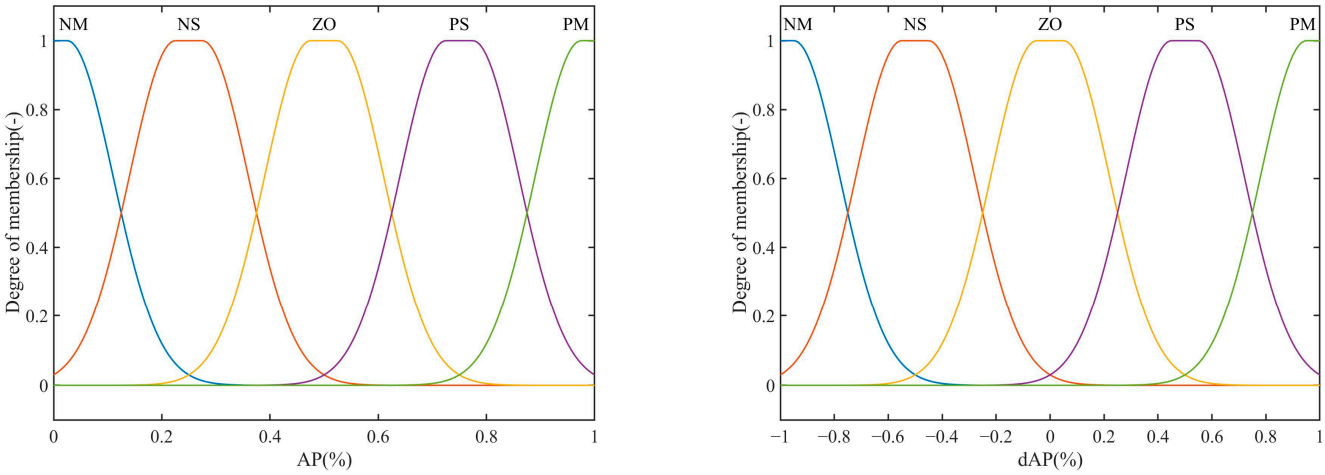

(**a**) Membership function for AP (**b**) Membership function for dAP

Figure 6. Membership functions for inputs.

Table 2. Fuzzy rules (γ).

dAP	*AP*				
	NM	**NS**	**ZO**	**PS**	**PM**
NM	NM	NM	NM	NS	ZO
NS	NM	NM	NS	ZO	PS
ZO	NM	NS	ZO	ZO	PS
PS	NM	NS	ZO	PS	PM
PM	NS	ZO	PS	PM	PM

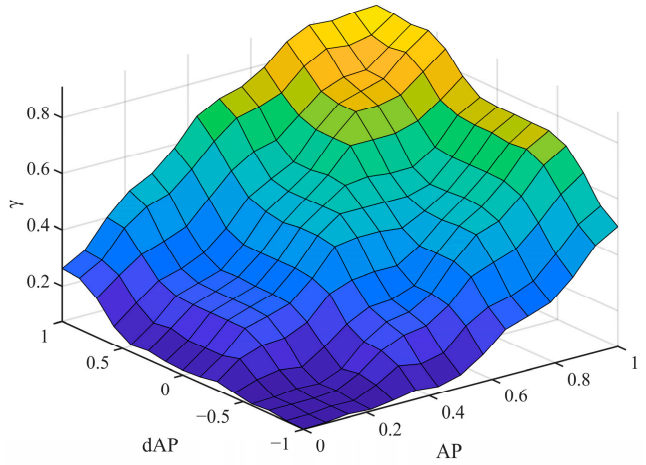

Figure 7. Output surface of the fuzzy inference system.

3.2. Improved Dynamic Programming Algorithm

3.2.1. Dynamic Programming

The objective of this economic velocity planning strategy is to solve the optimal control problem of a powertrain system with terminal constraints within a limited distance. During this process, the DP algorithm is employed, which is described in detail as follows:

The state variables are used to describe the states of each sub-stage, and the state of the k stage is denoted as $x(k), k = 1, 2, \cdots, N$, which belongs to the state space X. The decision variables are used to describe the control decisions that transfer the system from one sub-stage to the next, and the decision variable for the k stage is denoted as $u(k), k = 1, 2, \cdots, N-1$, which belongs to the decision space U. Both the state variable $x(k)$ and the control variable $u(k)$ are bounded and discrete, meaning they can take values within their respective domains. The state equation of this discrete system can be represented as

$$x(k+1) = f_x[x(k), u(k)] \tag{12}$$

The transition cost from the current state to the next state in each sub-stage is represented by a cost function, and the cost for the k stage is denoted as $L(k), k = 1, 2, \cdots, N-1$. It can be expressed as

$$L(k) = f_L[x(k), u(k)] \tag{13}$$

The cost function for the entire optimal control process can be expressed as

$$J = \sum_{k=1}^{N-1} L(k) + \xi[x(N)] \tag{14}$$

where $\xi[x(N)]$ represents the terminal cost of the system.

During the solving process, the backward induction starts from the N sub-stage, where the cost (terminal cost) of the N sub-stage can be represented as:

$$J^*[x(N)] = \xi[x(N)] \tag{15}$$

The optimal cost function for the k stage is $J^*[x(k)], k = 1, 2, \cdots, N-1$, which can be represented as

$$J^*[x(k)] = \min\{L(k) + J^*[x(k+1)]\} \tag{16}$$

After the backward induction is completed, for the control system with the initial state $x(1)$, the optimal cost function for the entire process is $J^*[x(1)]$, and the optimal control decision sequence is $u^* = \{u^*(1), u^*(2), \cdots, u^*(N-1)\}$.

The essence of solving the problem using the DP algorithm is to traverse all possible decisions of the state variables at each stage within the state space. It calculates the optimal decisions for all feasible states and stores them for direct table lookup, thereby avoiding redundant calculations. In the economic velocity planning for PHET, the original decision variables include gearbox gears, operating modes, and power allocation in different operating modes. Due to the complexity of the vehicle structure studied in this study, which includes four gearbox gears and three operating modes, using conventional DP algorithms to perform economic velocity planning would require traversing and solving for all the aforementioned factors as decision variables. This would exponentially increase the computational burden and significantly impact the efficiency of the algorithm.

In addition, in the conventional DP algorithm, the range of the state space and the discretization step size are fixed. However, velocity—as a state variable in economic velocity planning—has a significant range of fluctuations and is highly sensitive to temporal changes. If the conventional DP algorithm is used for economic velocity planning, there will be a large number of invalid state spaces and incorrect state transitions, which will affect the accuracy of the algorithm.

Therefore, it is necessary to optimize the DP algorithm before its application. The efficiency and accuracy of the DP algorithm depend on the number of state variables and decision variables, as well as the corresponding discrete grid. Since this study focuses on velocity planning, there is only one state variable, which is velocity. The optimization of the DP algorithm's efficiency and accuracy can be achieved by reducing the number of decision variables and dynamically adjusting the discrete grid, as well as limiting the state space.

3.2.2. Optimization of Decision Variables

The HET studied in this study has three operating modes: Single Electric Vehicle (SEV), Dual Electric Vehicle (DEV), and Hybrid Electric Vehicle (HEV). The operating modes of PHET are shown in Table 3. Additionally, the gearbox of the HET studied in this study consists of four gears. Due to the complexity of the operating modes and the vehicle structure, simplification is required before economic velocity planning. During the simplification process, both the vehicle's power performance and fuel economy need to be considered to allow the powertrain system to achieve optimal performance.

Table 3. The operating modes of PHET.

Operating Modes	MG1	MG2	Engine	BLM
SEV	×	√	×	√
DEV	√	√	×	√
HEV	√	√	√	×

Note: "√" represents that the power sources can work, or the BLM is locked; "×" represents that the power sources cannot work, or the BLM is released.

It can be seen from Table 3 that, in terms of power performance, the SEV mode exhibits the weakest power performance among the various operating modes, while the power

performance comparison between DEV and HEV varies depending on the gear position and vehicle velocity.

Figure 8 shows the comparison of the maximum acceleration of the vehicle on a straight road in the second gear. Before point A in the graph, DEV outperforms HEV in terms of power performance, while the opposite is true after that point. Additionally, due to the limitations imposed by the planetary gears structure and the maximum rotational speed of each power source, the maximum velocities differ between the DEV and the HEV in second gear, as indicated by segments B and C in Figure 8. Therefore, when shifting gear and selecting the operating mode, the power performance of each component in the powertrain system needs to be considered comprehensively.

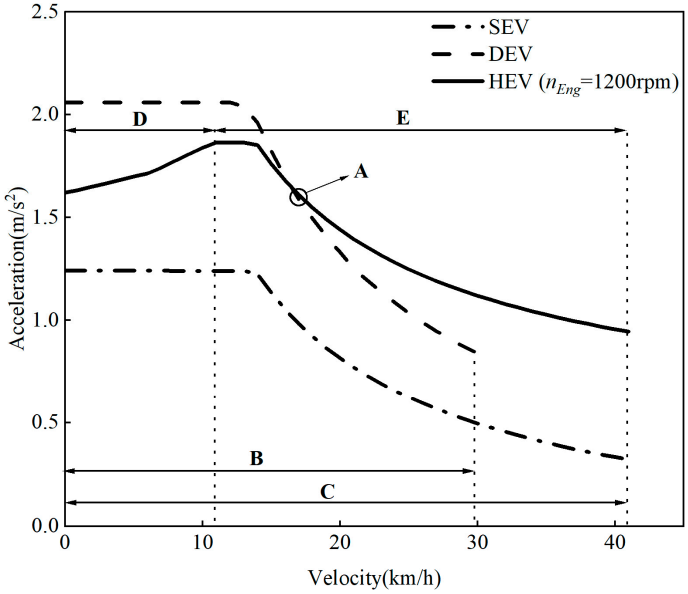

Figure 8. Acceleration comparison in second gear.

In terms of fuel economy, according to Figure 2, it can be observed that n_{Eng} exhibits better fuel economy around 1200 rpm when T_{Eng} is constant. Due to the characteristics of the dual planetary gears, in the HEV mode, the motor MG1 can control n_{Eng} at 1200 rpm to ensure relatively good fuel economy. When controlling n_{Eng} using MG1, based on the speed characteristics of PG1 (Equation (6)), the n_{MG1} can be expressed as

$$n_{MG1} = (1 + k_{p1}) \cdot n_{Eng} - k_{p1} \cdot n_{c1} \tag{17}$$

The n_{C1} can be expressed as

$$n_{C1} = \frac{30 \cdot v \cdot i_d \cdot i_g}{3.6 \cdot \pi \cdot R_{wh}} \tag{18}$$

According to Equations (17) and (18), it can be observed that n_{MG1} is negatively correlated with vehicle velocity (v) when n_{Eng} is fixed, with n_{MG1} increasing at lower v. Based on the external characteristic curve of MG1 (Figure 3), $\left|T_{MG1}^{Min}\right|$ decreases with an increase in n_{MG1} after reaching P_{MG1}^{Max}. Additionally, according to Equations (8)–(10), the maximum output torque ($T_{Eng\_out}^{Max}$) of the engine at this time can be expressed as:

$$T_{Eng\_out}^{Max} = \min\left[T_{Eng}^{Max}, (1 + k_{p1}) \cdot \left|T_{MG1}^{Min}\right|\right] \tag{19}$$

where, $T_{Eng\_out}^{Max}$ will be subject to restrictions imposed by $\left|T_{MG1}^{Min}\right|$ (segments D in Figure 8) and T_{Eng}^{Max} (segments E in Figure 8). In summary, in the HEV mode, the engine may not

be able to output maximum torque according to its external characteristics at lower v. Therefore, it is necessary to achieve a rational gear shifting and operating mode selection to ensure fuel economy while avoiding the occurrence of this problem.

In this study, to address the aforementioned issues, gear shifting and operating mode selection is correlated with the *AP* and velocity, as shown in Figure 9. The determination of gear shift velocity takes into account the speed characteristics (Table 1) of the electric motor and the engine, as well as the driver's driving behavior; and the determination of operating modes considers the speed and torque characteristics (Table 1) of the electric motor and the engine, as well as the driver's driving behavior.

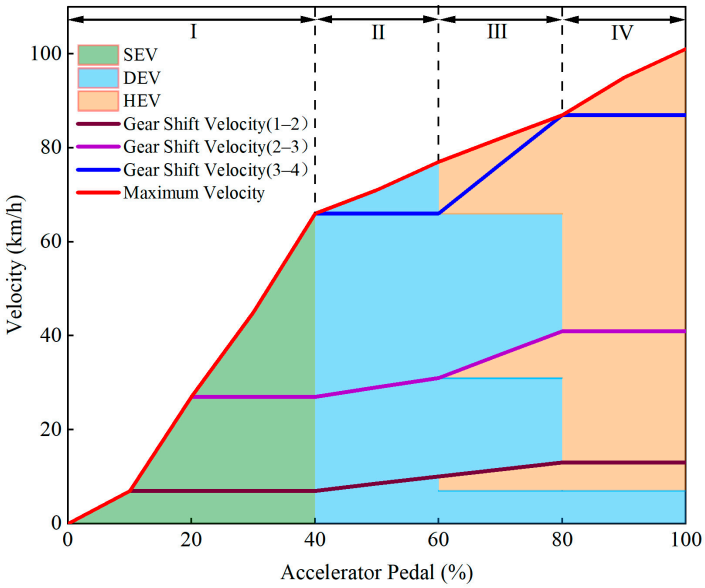

Figure 9. Gear shifting and operating mode selection.

By employing this approach, the computational efficiency of DP is improved by reducing the decision variables, while ensuring that the vehicle achieves optimal power performance when transitioning between different operating modes.

To differentiate between different driving styles, they can be classified based on the *AP* and operating modes. The specific classification (I to IV in Figure 9) is as follows:

I. Economical Driving (0–40%): In economical driving, the vehicle has relatively weak power demand. The HET operates only in the SEV, where only motor MG2 is engaged. There is no need to consider operating mode selection or power allocation during the drive.
II. Comfortable Driving (40–60%): In comfortable driving, the vehicle has moderate power demand. The HET operates only in the DEV mode, with both motor MG1 and motor MG2 engaged. There is no need to consider operating mode selection, but power allocation between the two motors needs to be taken into account.
III. Aggressive Driving (60–80%): In aggressive driving, the vehicle has strong power demand. The PHET alternates between the DEV and HEV, with a higher proportion in the DEV. Operating mode selection and power allocation between different components of the powertrain system need to be considered in this driving style.
IV. Dangerous Driving (80–100%): In dangerous driving, the vehicle has the strongest power demand. The driving situation of the PHET is similar to aggressive driving, but with a higher proportion of the HEV during this driving style. Additionally, when the vehicle's battery is low, gear shifting and operating mode selection will follow the rules of this driving style, although the power allocation strategy may differ.

3.2.3. Optimization of Step Size

When applying the DP algorithm to solve problems, it is common to divide the problem into multiple decision stages in the time domain, and then calculate the optimal performance indicators and decision variables for each sub-stage. In the context of economic velocity planning, the system disturbances are based on spatial factors such as road gradient and lane speed limits. If the optimization problem is discretized in the time domain, significant variations in vehicle velocity can occur in the spatial domain across different sub-stages, thereby affecting the planning results. Additionally, in this study, it is necessary to obtain road condition information ahead of time through V2X communication before conducting economic velocity planning.

Discretizing the optimization problem in the time domain alone would not accurately correspond the time domain to the spatial domain. Therefore, in this study, the DP algorithm based on spatial domain discretization is employed for the economic velocity planning strategy of the PHET. When determining the discretization step size $(\Delta s(k), k = 1, 2, \cdots, N-1)$ in the k stage, setting it as a constant value can lead to certain issues. For instance, if $\Delta s(k)$ is set to be too large, it can result in significant differences in velocity between adjacent nodes, thus impacting the accuracy of velocity planning and the effectiveness of the actual plans. On the other hand, if $\Delta s(k)$ is too small, it would require a larger number of steps in the planning space, thereby increasing the computational complexity. To effectively address this issue, this study sets $\Delta s(k)$ as a mathematical model that is correlated with the predicted velocity $v_p(k)$, and a gear adjustment factor $\chi_{gp}(k)$ in the k stage:

$$\Delta s(k) = v_p(k) \cdot \chi_{gp}(k), \chi_{gp}(k) \in (0.05, 0.1) \tag{20}$$

where $v_p(k)$ will be discussed in the next section, while $\chi_{gp}(k)$ is positively correlated with the predicted gear position.

3.2.4. Optimization of State Space

Before optimizing the DP algorithm's state space, it is necessary to determine the terminal state. In the context of economic velocity planning, the terminal state refers to the desired final vehicle velocity. The variation in vehicle velocity during travel is influenced by spatial domain information. Therefore, in the process of economic velocity planning, the terminal velocity is affected by the vehicle's current state, driver's driving style, and road information. In this study, the terminal velocity within each planning cycle is determined using a velocity prediction equation. It assumes that within each stage, the road slope and speed limit remain constant, and any variations in driving resistance due to changes in velocity are ignored. Additionally, the vehicle acceleration is assumed to be constant. The velocity prediction equation can be expressed as

$$v_p(k+1) = 3.6\sqrt{2 \cdot a_p(k) \cdot \Delta s(k) + \left[\frac{v_p(k)}{3.6}\right]^2} \tag{21}$$

where $a_p(k)$ is the predicted vehicle acceleration in the stage k. It can be expressed as:

$$a_p(k) = \frac{3.6}{\delta \cdot m \cdot R_{wh}} \left\{ F_p(k) - R_{wh}[F^p_{roll}(k) + F^p_{aero}(k) + F^p_{slope}(k)] \right\} \tag{22}$$

where $F^p_{roll}(k)$, $F^p_{air}(k)$, and $F^p_{gradiet}(k)$ represent the predicted rolling resistance, predicted air resistance, and predicted gradient resistance for the k stage, respectively. These values can be computed by incorporating road condition information obtained from V2X and Equation (11). $F_p(k)$ represents the predicted driving force on the tire in the k stage, and can be expressed as

$$F_p(k) = \gamma(k) \max\left[F^p_{out}(k)\right] \tag{23}$$

$$F_{out}^{p}(k) = \tau(k) \cdot T_{out}^{p}(k) \cdot i_{fd} \cdot i_g / R_{wh} \tag{24}$$

where $\tau(k)$ represents the torque relaxation factor, which is correlated with the driving style and road surface information. Its purpose is to avoid prolonged operation of the powertrain system under high-load conditions, which could impact the lifespan of the motor or engine. $T_{out}^{p}(k)$ represents the predicted torque output of the powertrain system during the k stage.

The constraint conditions are as:

$$\begin{cases} T_{MG1}^{Min} \le T_{MG1}^{p}(k) \le T_{MG1}^{Max}, T_{MG2}^{Min} \le T_{MG2}^{p}(k) \le T_{MG2}^{Max} \\ n_{MG1}^{Min} \le n_{MG1}^{p}(k) \le n_{MG1}^{Max}, n_{MG2}^{Min} \le n_{MG2}^{p}(k) \le n_{MG2}^{Max} \\ T_{Eng}^{Min} \le T_{Eng}^{p}(k) \le T_{Eng}^{Max} \\ P_{Batt}^{Min} \le P_{Batt}^{p}(k) \le P_{Batt}^{Max} \\ a_p^{Min} \le a_p(k) \le a_p^{Max} \\ \Delta s_{Min} \le \Delta s(k) \le \Delta s_{Max} \end{cases} \tag{25}$$

where T_{MG1}^{Min} and T_{MG2}^{Min} (T_{MG1}^{Max} and T_{MG2}^{Max}) are the minimum (maximum) output torques provided by motors MG1 and MG2, respectively. n_{MG1}^{Min} and n_{MG2}^{Min} (n_{MG1}^{Max} and n_{MG2}^{Max}) are the minimum (maximum) output speeds provided by motors MG1 and MG2, respectively. T_{Eng}^{Min} and T_{Eng}^{Max} are the minimum and maximum output torques, respectively, that are provided by the engine. P_{Batt}^{Min} and P_{Batt}^{Max} are the upper and lower limits of battery power, respectively. a_p^{Min} and a_p^{Max} are the minimum and maximum predicted acceleration, respectively. Δs_{Min} and Δs_{Max} are the minimum and maximum step size, respectively.

In the DP algorithm, the number of grid points is crucial in determining the computation results. Increasing the number of discrete grid points can lead to more accurate results, but a longer computation time. Conversely, reducing the number of grid points can yield faster computation results, but may introduce distortion in the obtained results. To address this issue, this study proposes an IDP algorithm that reduces grid points by constraining the state space without compromising the overall optimization performance. The principle is illustrated in Figure 10, where the discrete state variables of each stage on the spatial domain are transformed from the global state space (X_g) to a local predictive state space (X_{lp}). The spatial constraints consist of two boundary components, namely the predictive boundary (B_{pr}) and the planning boundary (B_{pl}). Among them, B_{pr} represents the boundaries predicted during the forecasting stage based on road information and driving style. The upper predictive boundary $B_{pr}^{u}(k+1), k = 1, 2, \cdots, N-1$ and the lower predictive boundary $B_{pr}^{l}(k+1), k = 1, 2, \cdots, N-1$ can be expressed as

$$B_{pr}^{u}(k+1) = f_{B_{pr}}\left\{ B_{pr}^{u}(k), \Delta s(k), \max\left[F_{out}^{p}(k) \right] \right\} \tag{26}$$

$$B_{pr}^{l}(k+1) = f_{B_{pr}}\left\{ B_{pr}^{l}(k), \Delta s(k), \min\left[F_{out}^{p}(k) \right] \right\} \tag{27}$$

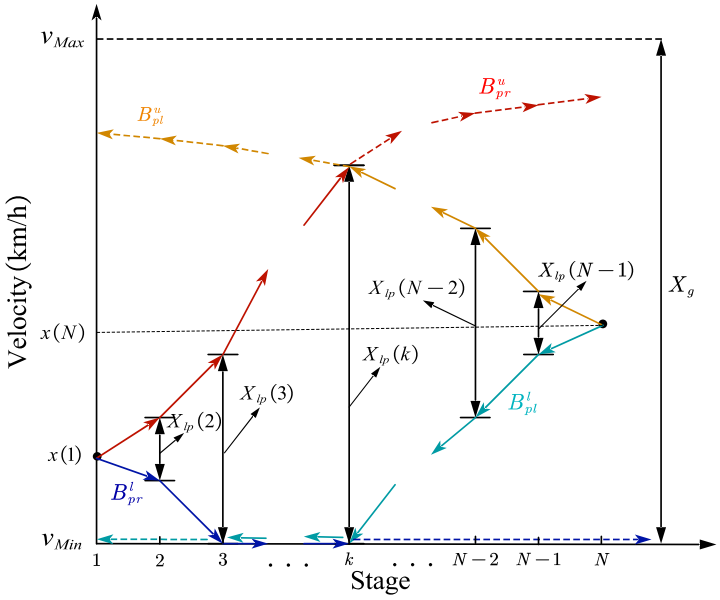

Figure 10. Optimization principle of constraining the state space.

The upper planning boundary $B^u_{pl}(k), k = 1, 2, \cdots, N-1$ and lower planning boundary $B^l_{pl}(k), k = 1, 2, \cdots, N-1$ are determined based on terminal velocity $x(N)$, and are calculated by reverse planning. They can be expressed as

$$B^u_{pl}(k) = f_{B_{pl}}\left\{B^u_{pl}(k+1), \Delta s(k), \min\left[F^p_{out}(k+1)\right]\right\} \tag{28}$$

$$B^l_{pl}(k) = f_{B_{pl}}\left\{B^l_{pl}(k+1), \Delta s(k), \max\left[F^p_{out}(k+1)\right]\right\} \tag{29}$$

Please refer to Equation (21) for the specific calculation method.

Combining $B_{pr}(k)$, $B_{pl}(k)$, AP, and road velocity limit (v^{road}_{Max} and v^{road}_{Min}), the $X_{lp}(k)$ for k stage in the IDP algorithm can be obtained. The upper bound $B_u(k), k = 2, \cdots, N-1$ and lower bound $B_l(k), k = 2, \cdots, N-1$ of $X_{lp}(k)$ can be expressed as:

$$B_u(k) = \min\left[B^u_{pr}(k), B^u_{pl}(k), v^{AP}_{Max}(k), v^{road}_{Max}(k)\right] \tag{30}$$

$$B_l(k) = \max\left[B^l_{pr}(k), B^l_{pl}(k), v^{road}_{Min}(k)\right] \tag{31}$$

where $v^{AP}_{Max}(k)$ represents the maximum vehicle velocity constrained by the accelerator pedal in the k stage, as referenced in Figure 9. $v^{road}_{Max}(k)$ and $v^{road}_{min}(k)$ are the maximum and minimum velocity limits of the road, respectively, which can be obtained through V2X.

By constraining the state space, the number of grid points can be effectively reduced. However, in this study, gear shifting and operating mode selection are based on the vehicle velocity and AP. Within the local predicted state space $X_{lp}(k)$, different gears and operating modes may be present. During the backward planning process, the vehicle state of the previous stage is derived from the vehicle state of the subsequent stage. This may lead to the situation where some state variables from the previous stage cannot be transferred to the subsequent stage during the forward transition, as shown in Figure 11.

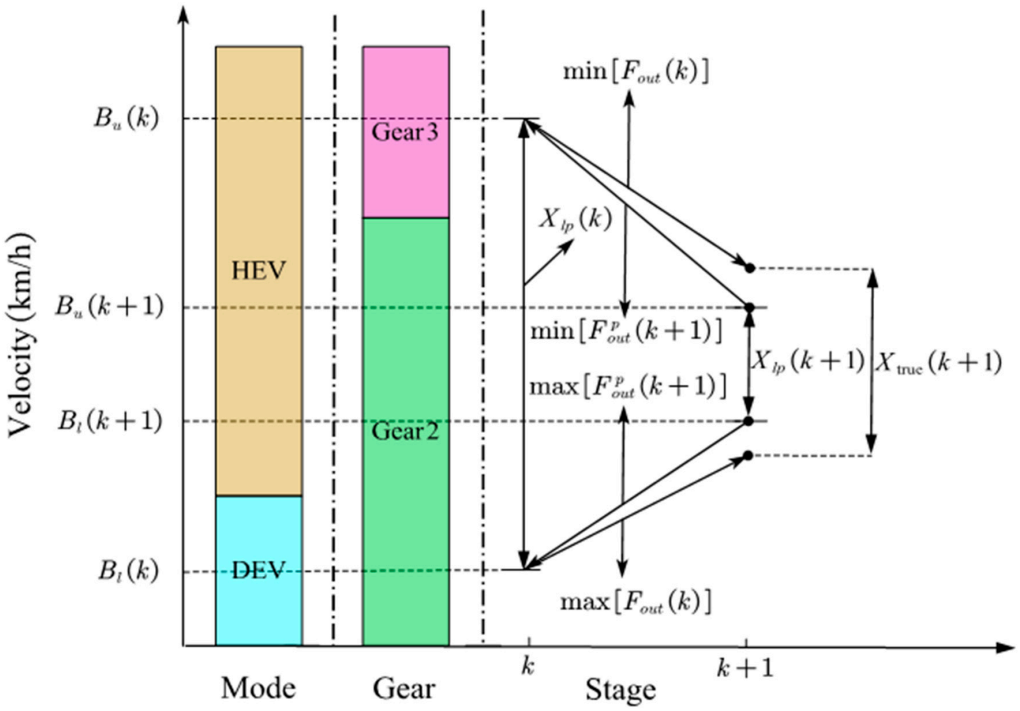

Figure 11. State transition from stage k to stage $k+1$.

In Figure 11, the $X_{lp}(k)$ of stage k is derived by backward propagation from $X_{lp}(k+1)$ of stage $k+1$. However, due to the differences in the vehicle's working mode and gear during forward transitions and backward propagation, there can be discrepancies between the true state space ($X_{true}(k+1)$) and $X_{lp}(k)$ of stage $k+1$. To address this issue, this study introduces a penalty function (φ) to adjust the cost function (L). The underlying principle can be expressed as

$$L_k(i,j) = \varphi_k[x(i), u(j)] \cdot L[x(i), u(j)] \tag{32}$$

where φ is dependent on the state variables $x(i), i = 1, 2, \ldots, N_X$ and control variables $u(j), j = 1, 2, \ldots, N_U$ at stage k. During the computation process of the IDP algorithm, if an infeasible state transition occurs, the introduction of the penalty function can significantly increase the overall cost. This allows for the avoidance of such situations in determining the optimal control decisions, and enhances the robustness of the algorithm during state transitions.

The optimized structure of the IDP algorithm, as shown in Figure 12, is presented in the previous sections. In this figure, N represents the number of stages in each planning cycle, N_X denotes the number of discrete state variables, N_U represents the number of discrete decision variables, X_{grid} represents the discrete state variable function, U_{grid} represents the discrete decision variable function, L represents the cost function of each sub-stage, and J represents the overall cost function.

Firstly, the terminal velocity $x(N)$ and step sizes Δs for each substage are obtained through predictive calculations. Secondly, the boundaries $B_u(k)$ and $B_l(k)$ are estimated using forward prediction and backward planning. Thirdly, $X_{lp}(k)$, which satisfies the imposed constraints, is discretized to obtain $X^{(i)}_{grid}(k)$. Based on the characteristics of $X^{(i)}_{grid}(k)$, $U^{(J)}_{grid}(k,i)$ is determined. Subsequently, $X^{(i)}_{grid}(k)$ is reevaluated to determine its capability to successfully accomplish the state transition. If it cannot do so, the cost at that moment is amplified through the use of a penalty function ($\gamma^{(i,j)}(k)$). Finally, the minimum $J^{(I)}(k)$ in this state is calculated.

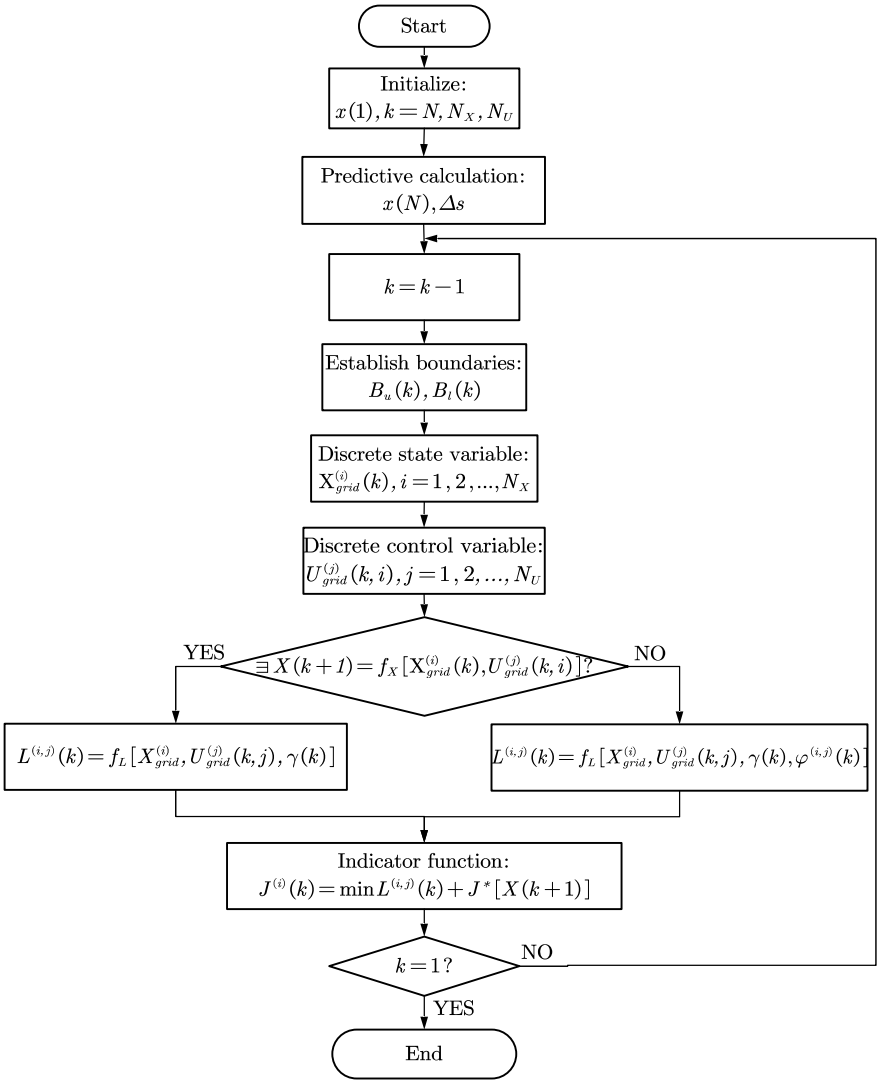

Figure 12. Optimized structure of the IDP algorithm.

3.3. Economy Velocity Planning Strategy Based on Driving Style and IDP

In this section, an economy velocity planning strategy based on driving style and the IDP algorithm (EVPS-DSIDP) is proposed to address the economic velocity planning problem while driving under different driving styles (Figure 13).

In EVPS-DSIDP, the driving style is first identified based on driver behavior (*AP* and *dAP*). Subsequently, the IDP algorithm is employed for offline iterative optimization to obtain the optimal velocity trajectory under the current driving conditions. Finally, the optimized results are applied to an online EMS to dynamically solve the optimal control problem in real-time.

Given the determination of driving style and road information, the variation of vehicle velocity and the power allocation between the electric motor and the engine constitute a typical multi-objective optimization problem. The PHET studied in this study is a type of commercial vehicle, where the focus of optimization lies in prioritizing fuel consumption, battery energy consumption, and travel time. Under the assumption of neglecting battery life degradation and component wear, both battery energy consumption and engine fuel consumption can be regarded as economic costs, while travel time and acceleration can be considered as power performances. The objective of this study is to construct a multi-objective optimization problem with the optimization targets of economic costs and power performances.

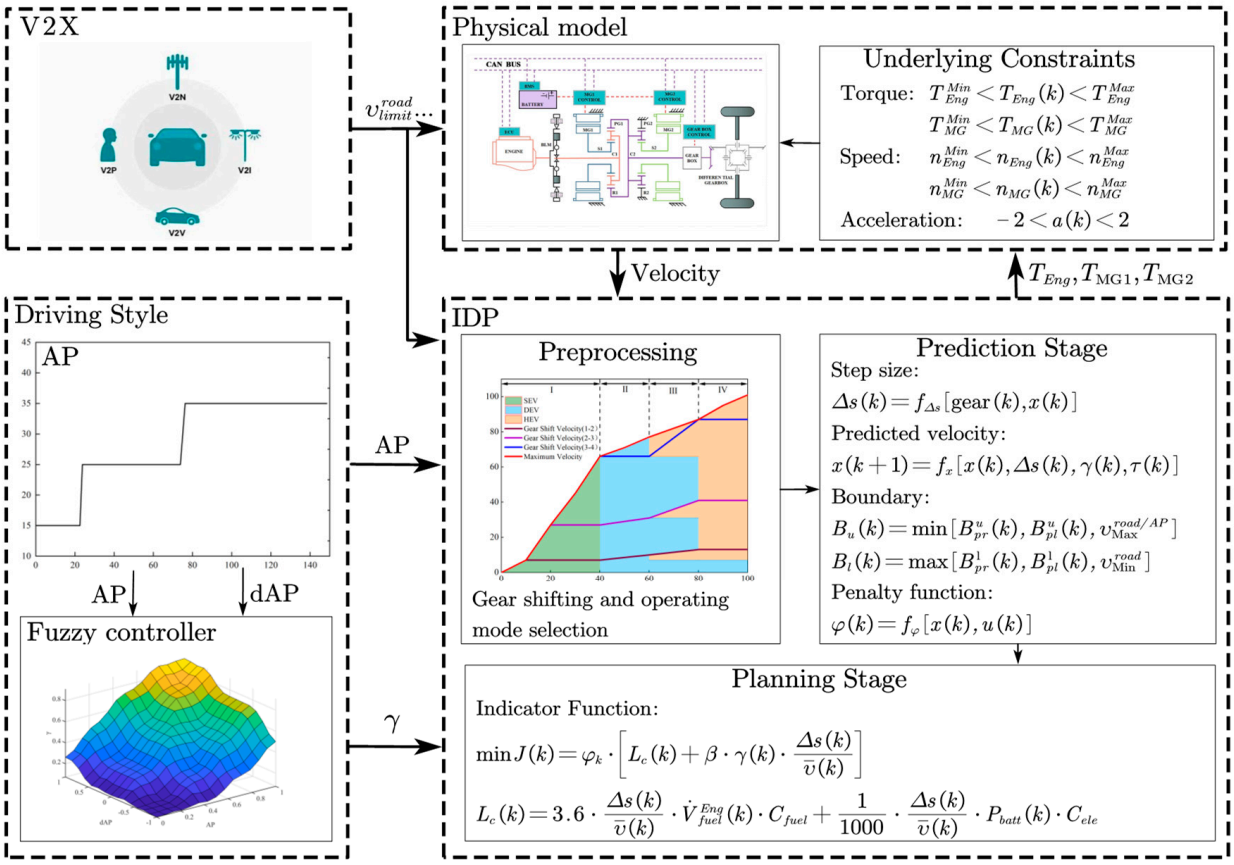

Figure 13. Logic diagram of EVPS-DSIDP.

In summary, when constructing the optimal control problem, the fuel consumption of the engine, battery energy consumption, and travel time are all considered as cost functions. Firstly, to account for power dynamics, a power coefficient (γ) is introduced to dynamically adjust the weight of power cost. Secondly, due to the significant difference in magnitude between economic cost and travel time cost, a cost weighting factor (β) is introduced to adjust this disparity. Finally, a penalty function (φ) is introduced to ensure the correct transition of state variables. The objective function of this multi-objective optimization optimal control problem can be expressed as:

$$\min J = \varphi \cdot (L_c + \beta \cdot \gamma \cdot t) \tag{33}$$

By transforming Equation (33) into a discrete form with respect to distance, the optimal indicator function can be expressed as:

$$\min J(k) = \varphi_k \cdot \left[L_c(k) + \beta \cdot \gamma(k) \cdot \frac{\Delta s(k)}{\overline{v}(k)} \right] \tag{34}$$

where $L_c(k)$ represents the economic costs of stage k, which can be expressed as:

$$L_c(k) = 3.6 \cdot \frac{\Delta s(k)}{\overline{v}(k)} \cdot \dot{V}_{fuel}^{Eng}(k) \cdot C_{fuel} + \frac{1}{1000} \cdot \frac{\Delta s(k)}{\overline{v}(k)} \cdot P_{batt}(k) \cdot C_{ele} \tag{35}$$

where $\overline{v}(k)$ represents the predicted average velocity of stage k, which can be expressed as:

$$\overline{v}(k) = \frac{1}{2}[v(k+1) + v(k)] \tag{36}$$

In addition, the consideration of driving and ride comfort, as well as vehicle acceleration and deceleration performance, is required for power cost analysis. Excessive acceleration can decrease driving and ride comfort and may also increase economic costs. Similarly, excessive deceleration can negatively impact the driving experience and energy recovery efficiency. Therefore, it is necessary to impose reasonable constraints on vehicle acceleration. Taking into account driving safety, comfort, economic costs, and travel time costs, the acceleration constraints for each stage can be determined as follows:

$$-2 \leq a(k) \leq 2 \tag{37}$$

The constraint conditions are as follows:

$$\begin{cases} T_{MG1}^{Min} \leq T_{MG1}(k) \leq T_{MG1}^{Max}, T_{MG2}^{Min} \leq T_{MG2}(k) \leq T_{MG2}^{Max} \\ n_{MG1}^{Min} \leq n_{MG1}(k) \leq n_{MG1}^{Max}, n_{MG2}^{Min} \leq n_{MG2}(k) \leq n_{MG2}^{Max} \\ T_{Eng}^{Min} \leq T_{Eng}(k) \leq T_{Eng}^{Max}, n_{Eng}^{Min} \leq n_{Eng}(k) \leq n_{Eng}^{Max} \\ P_{Batt}^{Min} \leq P_{Batt}(k) \leq P_{Batt}^{Max} \\ -2 \leq a(k) \leq 2 \end{cases} \tag{38}$$

4. Simulation Results and Analysis

To validate the effectiveness of the proposed EVPS-DSIDP, this study conducts a comparative analysis with three other control strategies. The analysis examines the velocity variation during initial acceleration on a flat road (with sufficient SOC) under different control strategies, as well as the associated economic cost and travel time required for simulation. A lower economic cost and travel time indicate better economy and power performance. Furthermore, considering that shifting conditions, operating modes, and maximum vehicle velocities differ across various driving styles, to enhance the robustness of the simulation results, the simulation conditions are set to include continuous driving over three planning cycles under different driving styles.

The selected comparative control strategies are as follows: rule-based constant acceleration control strategy (CACS-RB), economy optimization control strategy based on IDP (EOCS-IDP), and power optimization control strategy based on IDP (POCS-IDP). The characteristics of these three strategies are as follows:

I. CACS-RB: Under this strategy, the velocity changes uniformly within each planning cycle, and the primary power source during driving is the motor MG2. Only when the power of motor MG2 is insufficient will the engine or motor MG1 participate. This strategy serves as the main control group.
II. EOCS-IDP: Under this strategy, the velocity planning only considers economy, with the primary goal of minimizing economic cost.
III. POCS-IDP: Under this strategy, the velocity planning considers both economy and power performance, but with a greater emphasis on power performance.

4.1. Simulation Results

4.1.1. Economical Driving

Figure 14 shows the impact of different control strategies on the velocity during economical driving, I to III represent three driving stages. In economical driving, only motor MG2 is involved, and the torque and efficiency of MG2 during its operation are shown in Figure 15. The economic cost and travel time under different stages are presented in Table 4.

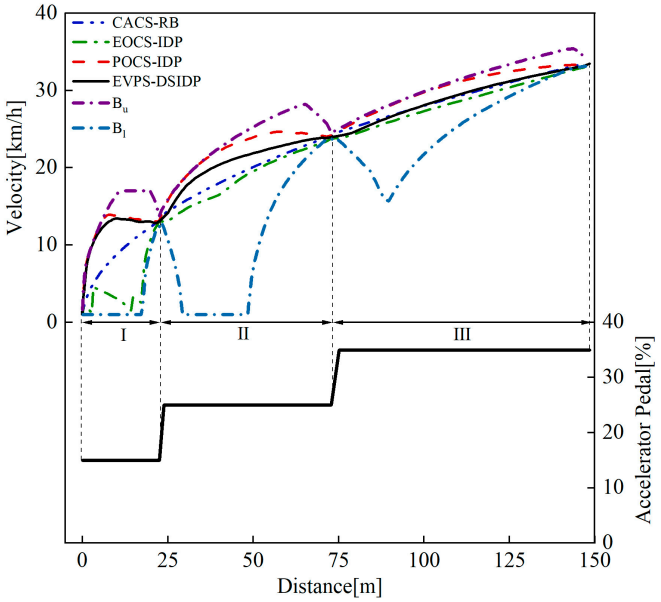

Figure 14. Velocity and accelerator pedal in economical driving.

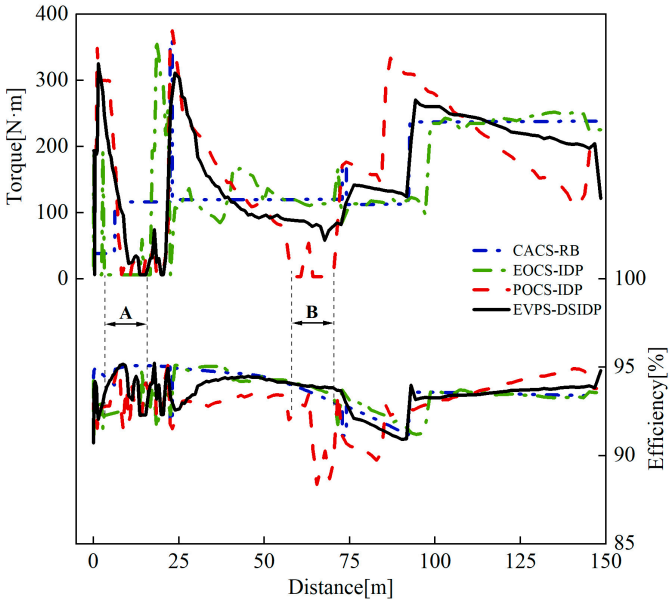

Figure 15. Torque and efficiency of MG2 in economical driving.

Table 4. The Total Cost of Economical Driving.

Strategy	Stages					
	I		II		III	
	Cost (RMB)	Time (s)	Cost (RMB)	Time (s)	Cost (RMB)	Time (s)
CAC-RB	0.1031	11.47	0.2476	9.58	0.3439	9.27
EO-IDP	0.0884	25.53	0.2369	10.07	0.3364	9.64
PO-IDP	0.102	6.98	0.2497	8.34	0.3440	8.91
EVPS-DSIDP	0.1012	7.59	0.2449	9.09	0.3392	9.47

In Segment I of Figure 14, EOCS-IDP adopts a strategy of accelerating and then decelerating to reduce economic cost and optimize economy. At this time, T_{MG2} and η_{MG2} are as shown in Segment A of Figure 15. Although EOCS-IDP achieves relatively good

optimization in terms of economy, it overlooks power optimization due to excessive pursuit of economy, resulting in a significant increase in travel time compared to CACS-RB, and ultimately leads to suboptimal results. In Segment II of Figure 14, POCS-IDP also exhibits the acceleration-deceleration pattern. This is because the initial power in the planning cycle is too strong, requiring deceleration in the later stage to achieve the target velocity. The T_{MG2} during deceleration is shown in Segment B of Figure 15. Similar situations occur in other driving styles, which are not repeated in the following text. This strategy has the best power optimization among the various strategies but lacks satisfactory economy optimization due to an excessive focus on power optimization. In contrast, the proposed EVPS-DSIDP in this study achieves a more balanced improvement in both power and economy by identifying the driving style.

4.1.2. Comfortable Driving

Figure 16 shows the impact of different control strategies on the velocity during comfortable driving, I to III represent three driving stages. In comfortable driving, both motor MG1 and motor MG2 are involved, and their torque and efficiency during operation are shown in Figures 17 and 18, respectively. The economic cost and travel time under different stages are presented in Table 5. In Segment I of Figure 17, EOCS-IDP also exhibits the acceleration-deceleration pattern, but due to the higher target velocity, the distance of deceleration coasting is smaller compared to economical driving. From Figures 17 and 18, it can be observed that, compared to EOCS-IDP and EVPS-DSIDP, the motors MG1 and MG2 under the POCS-IDP strategy operate in areas with lower efficiency to pursue stronger power. On the other hand, the motor efficiency is the poorest in CACS-RB without velocity planning, which further demonstrates the practicality of conducting economy velocity planning.

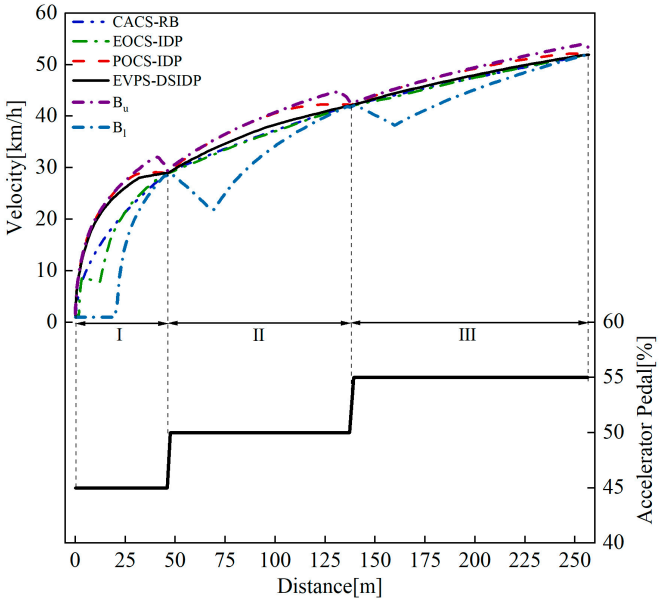

Figure 16. Velocity and accelerator pedal in comfortable driving.

4.1.3. Aggressive Driving

Figure 19 shows the impact of different control strategies on the velocity during aggressive driving, I to III represent three driving stages. In aggressive driving, both motor MG1, motor MG2, and the engine are involved, and their torque and efficiency/BSFC during operation are shown in Figures 20–22 respectively. The economic cost and travel time under different stages are presented in Table 6. The vehicle operates alternately in DEV and HEV, as illustrated in Figure 9.

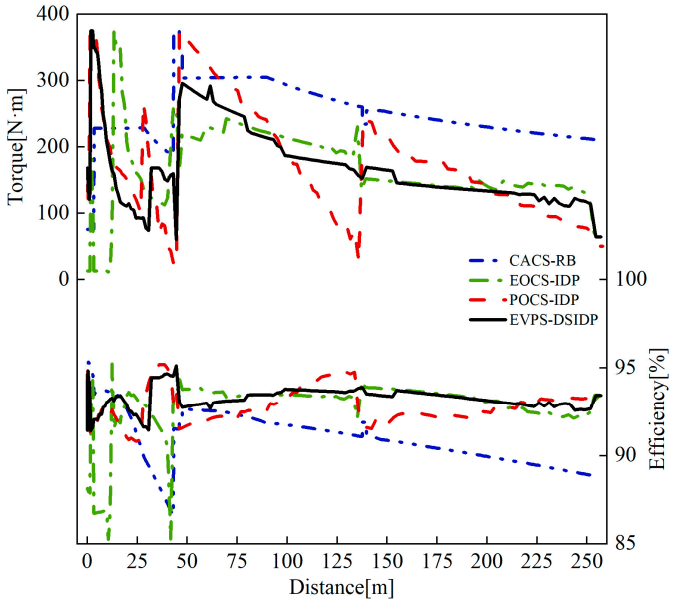

Figure 17. Torque and efficiency of MG2 in comfortable driving.

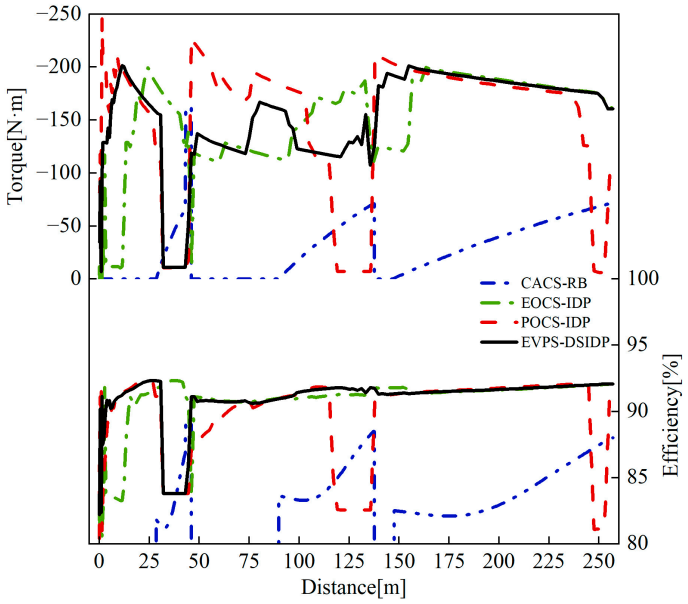

Figure 18. Torque and efficiency of MG1 in comfortable driving.

Table 5. The Total Cost of Comfortable Driving.

Strategy	Stages					
	I		II		III	
	Cost (RMB)	Time (s)	Cost (RMB)	Time (s)	Cost (RMB)	Time (s)
CAC-RB	0.4307	11.06	0.5489	9.27	0.6130	9.15
EO-IDP	0.4093	15.92	0.5364	9.29	0.5916	9.14
PO-IDP	0.4224	8.03	0.5515	8.76	0.6017	8.94
EVPS-DSIDP	0.4199	8.28	0.5416	9.09	0.5929	9.08

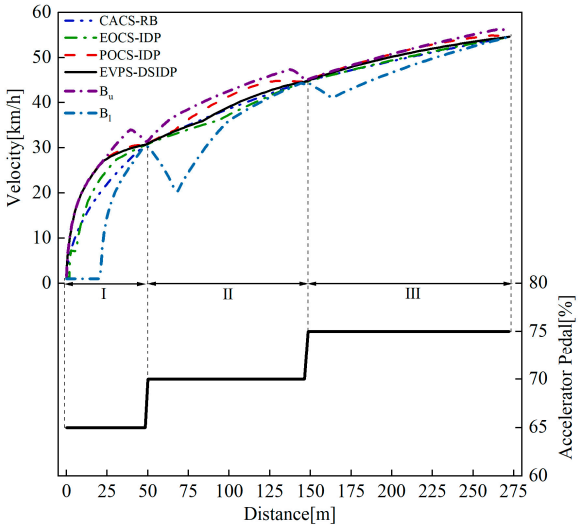

Figure 19. Velocity and accelerator pedal in aggressive driving.

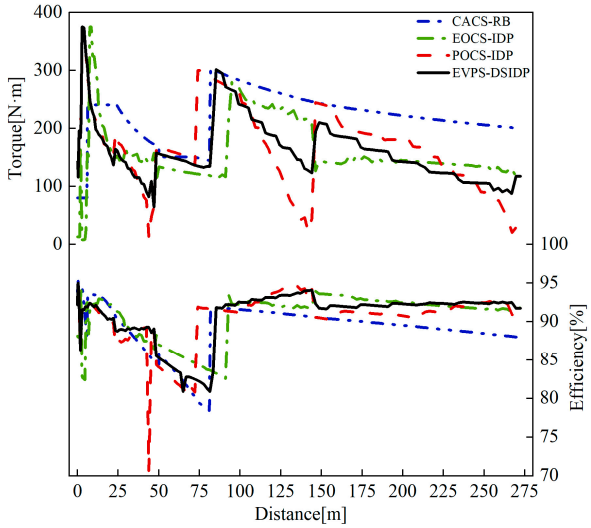

Figure 20. Torque and efficiency of MG2 in aggressive driving.

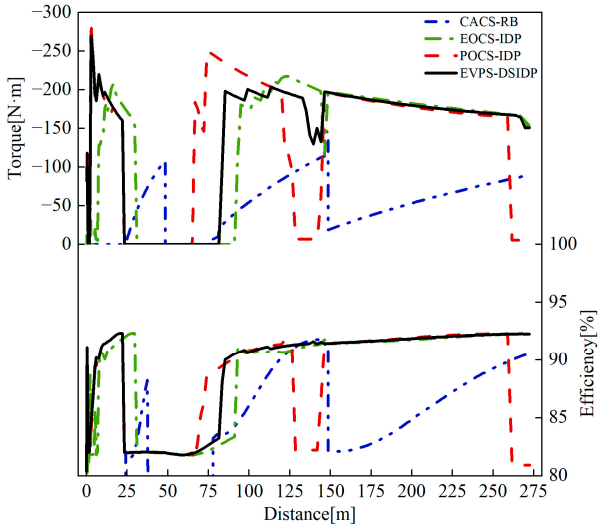

Figure 21. Torque and efficiency of MG1 in aggressive driving.

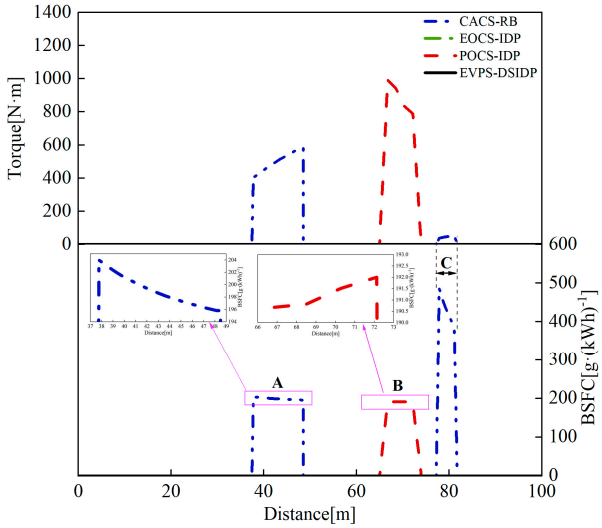

Figure 22. Torque and BSFC of engine in aggressive driving.

Table 6. The Total Cost of Aggressive Driving.

Strategy	Stages					
	I		II		III	
	Cost (RMB)	Time (s)	Cost (RMB)	Time (s)	Cost (RMB)	Time (s)
CAC-RB	0.5038	11.02	0.6438	9.35	0.6589	9.14
EO-IDP	0.4655	14.44	0.6248	9.53	0.6295	9.10
PO-IDP	0.4843	8.16	0.6490	8.98	0.6424	8.93
EVPS-DSIDP	0.4823	8.19	0.6399	9.30	0.6360	9.02

The power distribution between the motor and engine, whether in DEV or HEV, needs to consider overall cost, road information, and vehicle status. Taking the HEV mode in this simulation as an example, the planning results of EOCS-IDP and EVPS-DSIDP indicate that during this period, minimizing overall cost requires the engine to be inactive. However, due to the stronger power demand in POCS-IDP, there are certain moments in the simulation where the engine needs to participate, as indicated by the BSFC of the engine in Figure 22, Segment B. Additionally, the BSFC of the engine under CACS-RB is shown in Figure 22, Segments A and C. It can be observed from the figures that the engine's BSFC is significantly lower under POCS-IDP compared to CACS-RB.

4.1.4. Dangerous Driving

Figure 23 shows the impact of different control strategies on the velocity during dangerous driving, I to III represent three driving stages. In dangerous driving, motor MG1, motor MG2, and the engine are all involved, and their torque and efficiency/BSFC during operation are shown in Figures 24–26 respectively. The economic cost and travel time under different stages are presented in Table 7. Compared to aggressive driving, the vehicle operates more in hybrid mode during dangerous driving, and the driver has a stronger intention for acceleration. Due to the higher target speed obtained through prediction in this driving style, EOCS-IDP no longer exhibits the acceleration followed by deceleration pattern, as indicated in Figure 23. It can be observed from Figure 23 that the economically planned velocities by EOCS-IDP and EVPS-DSIDP are similar, indicating that under this driving style, EOCS-IDP and EVPS-DSIDP yield similar optimal controls.

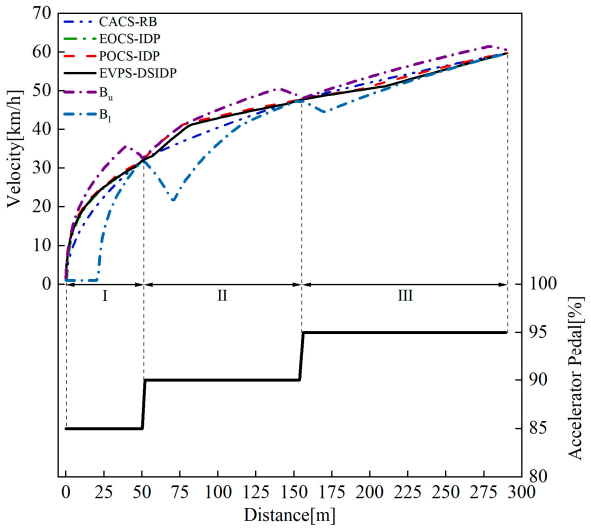

Figure 23. Velocity and accelerator pedal in dangerous driving.

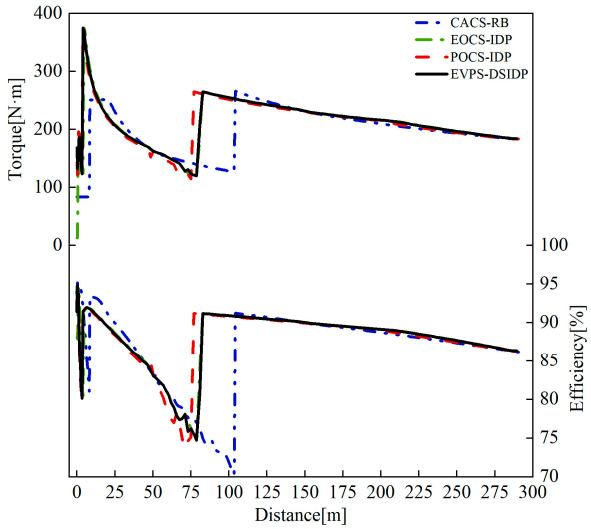

Figure 24. Torque and efficiency of MG2 in dangerous driving.

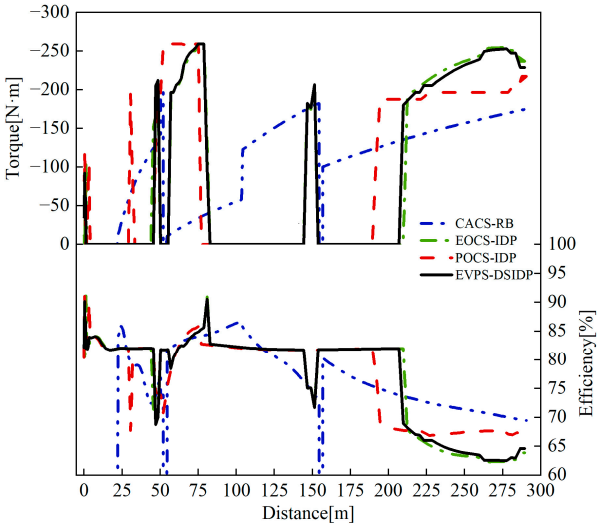

Figure 25. Torque and efficiency of MG1 in dangerous driving.

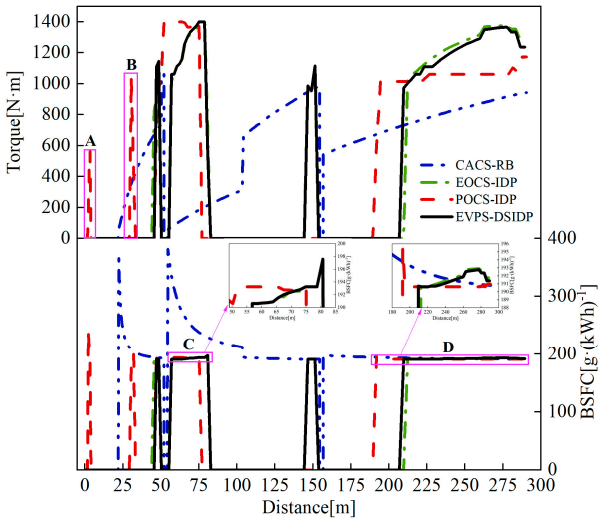

Figure 26. Torque and BSFC of MG2 in dangerous driving.

Table 7. The Total Cost of Dangerous Driving.

Strategy	Stages					
	I		II		III	
	Cost (RMB)	Time (s)	Cost (RMB)	Time (s)	Cost (RMB)	Time (s)
CAC-RB	0.5811	10.96	0.9272	9.35	1.0035	9.12
EO-IDP	0.5382	10.63	0.8553	8.99	0.9786	9.27
PO-IDP	0.5544	8.72	0.8647	8.86	0.9901	9.19
EVPS-DSIDP	0.5397	8.90	0.8609	8.99	0.9830	9.26

However, due to the stronger power demand in POCS-IDP, there are instances of brief engine start-stop during the planning process, as shown in Segments A and B of Figure 26, which is undesirable in practice. In this driving style, motor MG1 is mainly used to regulate the engine operating point, thus its torque variation trend is similar to that of the engine. Additionally, from the BSFC variation curve in Figure 26 (Segments C and D), it can be observed that reasonable velocity planning enables the engine to operate in a more efficient region.

4.2. Analysis

Due to slight differences in the starting and ending velocities of different strategies within a single planning cycle, there may be deviations in the results. In order to provide a more comprehensive comparison of the power and economy optimization effects of different control strategies, Figure 27 displays the required economic cost and travel time after accelerating for three planning cycles under different driving styles, and under the same conditions.

From the simulation results, it can be concluded that

I. In economical driving, compared to CACS-RB, both EOCS-IDP and EVPS-DSIDP can reduce economic costs by 4.29% and 1.32%, respectively. However, due to EOCS-IDP's excessive pursuit of economic optimization, it leads to an increase in travel time by 49.18%. On the other hand, POCS-IDP effectively optimizes power, resulting in a 20.07% reduction in travel time, but with a slight increase in economic costs by 0.16%. In contrast, by identifying the driving styles, EVPS-DSIDP achieves a 13.75% reduction in travel time while decreasing economic costs.
II. In comfortable driving, comparing CACS-RB to EOCS-IDP, POCS-IDP, and EVPS-DSIDP, they can all reduce economic costs by 3.48%, 1.07%, and 2.40%, respectively. Although EOCS-IDP achieves the best optimization in terms of economy, it results in a

16.57% increase in travel time. In this driving style, both POCS-IDP and EVPS-DSIDP can reduce travel time while lowering economic costs, with travel time reductions of 12.71% and 10.25%, respectively.

III. In aggressive driving, the optimization in terms of economy is slightly higher compared to comfortable driving. Comparing CACS-RB to EOCS-IDP, POCS-IDP, and EVPS-DSIDP, they can all reduce economic costs by 4.80%, 1.71%, and 2.68%, respectively. However, EOCS-IDP increases travel time by 12.08% while POCS-IDP and EVPS-DSIDP decrease travel time by 11.68% and 10.68%, respectively.

IV. In dangerous driving, comparing CACS-RB to EOCS-IDP, POCS-IDP, and EVPS-DSIDP, they can all reduce economic costs while decreasing travel time. The reduction in economic costs is 5.36%, 4.36%, and 5.10%, respectively, while the reduction in travel time is 1.82%, 8.97%, and 7.73%, respectively.

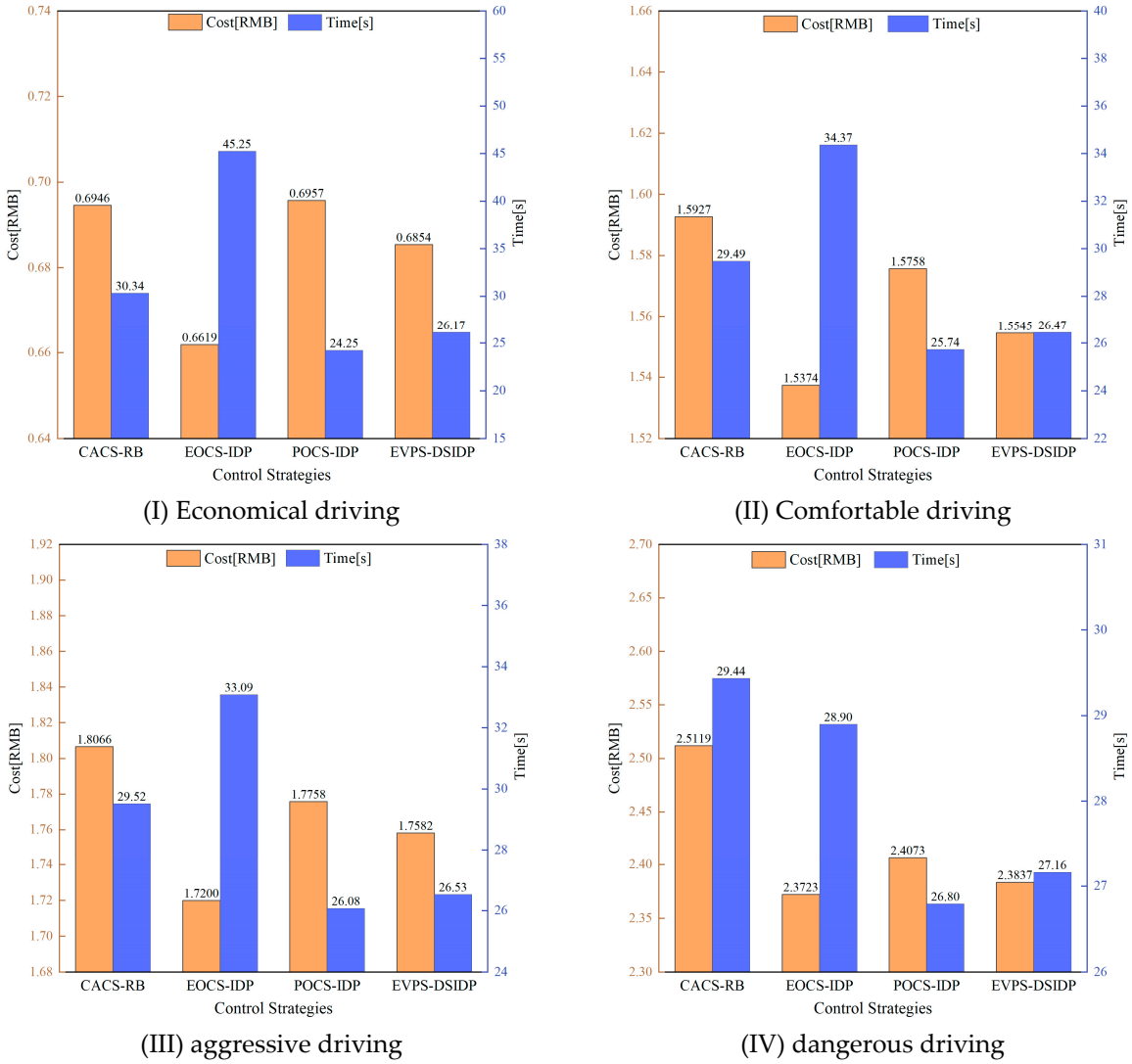

(I) Economical driving (II) Comfortable driving

(III) aggressive driving (IV) dangerous driving

Figure 27. Economic cost and travel time under different driving styles.

From the simulation results, it can be concluded that

I. In economical driving, compared to CACS-RB, both EOCS-IDP and EVPS-DSIDP can reduce economic costs by 4.29% and 1.32%, respectively. However, due to EOCS-IDP's excessive pursuit of economic optimization, it leads to an increase in travel time by 49.18%. On the other hand, POCS-IDP effectively optimizes power, resulting in a 20.07% reduction in travel time, but with a slight increase in economic costs by

0.16%. In contrast, by identifying the driving styles, EVPS-DSIDP achieves a 13.75% reduction in travel time while decreasing economic costs.

II. In comfortable driving, comparing CACS-RB to EOCS-IDP, POCS-IDP, and EVPS-DSIDP, they can all reduce economic costs by 3.48%, 1.07%, and 2.40%, respectively. Although EOCS-IDP achieves the best optimization in terms of economy, it results in a 16.57% increase in travel time. In this driving style, both POCS-IDP and EVPS-DSIDP can reduce travel time while lowering economic costs, with travel time reductions of 12.71% and 10.25%, respectively.

III. In aggressive driving, the optimization in terms of economy is slightly higher compared to comfortable driving. Comparing CACS-RB to EOCS-IDP, POCS-IDP, and EVPS-DSIDP, they can all reduce economic costs by 4.80%, 1.71%, and 2.68%, respectively. However, EOCS-IDP increases travel time by 12.08% while POCS-IDP and EVPS-DSIDP decrease travel time by 11.68% and 10.68%, respectively.

IV. In dangerous driving, comparing CACS-RB to EOCS-IDP, POCS-IDP, and EVPS-DSIDP, they can all reduce economic costs while decreasing travel time. The reduction in economic costs is 5.36%, 4.36%, and 5.10%, respectively, while the reduction in travel time is 1.82%, 8.97%, and 7.73%, respectively.

During the simulation process, the selection of the power coefficient (γ) is a key factor in obtaining different simulation results. For EOCS-IDP and POCS-IDP, γ is set to 0 and 1, respectively, representing the absence of power optimization and a strong emphasis on power optimization. In the case of EVPS-DSIDP, the γ is determined through the identification of driving styles, as shown in Figure 28.

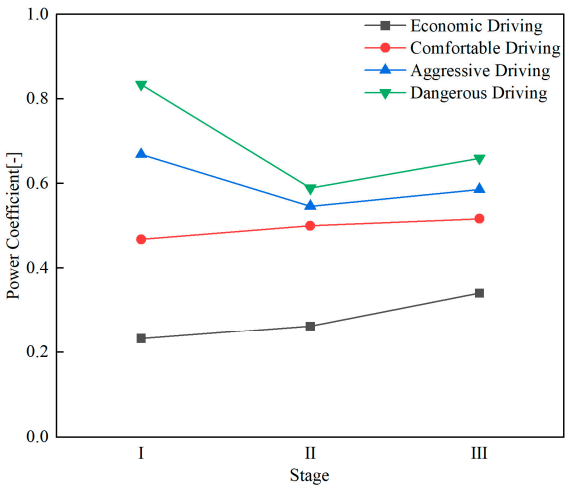

Figure 28. The power coefficient of EVPS-DSIDP under different driving styles.

From Figure 28, it can be observed that the value of γ under EVPS-DSIDP varies across different planning cycles for different driving styles. Since in this study, *AP* is varied starting from 0 in each simulation, the initial *dAP* is significant (65% and 85%) for aggressive and dangerous driving, respectively. This results in a larger power coefficient in the first stage compared to the subsequent stages, thereby demonstrating the effectiveness of fuzzy control.

5. Conclusions

To enhance the fuel economy and performance of PHET, this study proposes an economic velocity planning strategy based on driving style and IDP algorithm: EVPS-DSIDP. The feasibility and effectiveness of the proposed strategy are validated through simulation tests under different driving styles. The main tasks include:

First, in this study, the correlation between gear shifting and operating mode selection with accelerator pedal and vehicle velocity is established. While ensuring good fuel

economy and performance during vehicle operation, the computational efficiency of the DP algorithm is improved by reducing the decision variables. Secondly, the computational efficiency and accuracy of the DP algorithm are enhanced by dynamically adjusting the discretization step and constraining the state space. Simultaneously, a penalty function was introduced in the calculations to enhance the robustness of state transitions. Finally, a fuzzy controller is utilized to process the accelerator pedal information and obtain the power coefficient, which dynamically addresses the performance optimization objective of the vehicle under different driving styles. In different driving styles, compared to CACS-RB, EVPS-DSIDP exhibited an average reduction of 2.88% and 10.6% in economic costs and travel time, respectively. Compared to EOCS-IDP, EVPS-DSIDP exhibited an average reduction of nearly 22.75% in travel time. Compared to POCS-IDP, EVPS-DSIDP exhibited an average reduction of nearly 1.19% in economic costs.

In the future, the proposed strategy will be validated in actual vehicles, and the impact of SOC and complex road conditions on the economic velocity planning strategy will be investigated.

Author Contributions: Conceptualization, Y.L. and R.Y.; methodology, Y.L.; software, Y.L.; validation, Y.L. and Z.W.; formal analysis, Y.L. and R.Y; investigation, M.X. and W.H.; resources, Y.L., R.Y. and W.H.; data curation, Y.L. and Z.W.; writing—original draft preparation, Y.L.; writing—review and editing, Y.L.; visualization, Y.L.; supervision, R.Y.; project administration, W.H.; funding acquisition, W.H. All authors have read and agreed to the published version of the manuscript.

Funding: This research was funded by the Science and Technology Major Project of Guangxi, China, grant number AA22068062 and AA22068061.

Data Availability Statement: Not applicable.

Conflicts of Interest: The authors declare no conflict of interest.

References

1. Xu, F.; Crawford, C.; Feng, Y.; Lin, Z.; Li, S. Environment-economic analysis of diesel, hybrid electric, plug-in hybrid electric trucks in China. *Transp. Res. Part D Transp. Environ.* **2023**, *117*, 103661. [CrossRef]
2. Xue, Q.; Zhang, X.; Teng, T.; Zhang, J.; Feng, Z.; Lv, Q. A Comprehensive Review on Classification, Energy Management Strategy, and Control Algorithm for Hybrid Electric Vehicles. *Energies* **2020**, *13*, 5355. [CrossRef]
3. Zhu, Y.; Li, X.; Liu, Q.; Li, S.; Xu, Y. Review article: A comprehensive review of energy management strategies for hybrid electric vehicles. *Mech. Sci.* **2022**, *13*, 147–188. [CrossRef]
4. Khayyam, H.; Bab-Hadiashar, A. Adaptive intelligent energy management system of plug-in hybrid electric vehicle. *Energy* **2014**, *69*, 319–335. [CrossRef]
5. Bingzhan, Z.; Mi, C.C.; Mengyang, Z. Charge-Depleting Control Strategies and Fuel Optimization of Blended-Mode Plug-In Hybrid Electric Vehicles. *IEEE Trans. Veh. Technol.* **2011**, *60*, 1516–1525. [CrossRef]
6. Li, X.; Evangelou, S.A. Torque-Leveling Threshold-Changing Rule-Based Control for Parallel Hybrid Electric Vehicles. *IEEE Trans. Veh. Technol.* **2019**, *68*, 6509–6523. [CrossRef]
7. Farhadi Gharibeh, H.; Farrokhifar, M. Online Multi-Level Energy Management Strategy Based on Rule-Based and Optimization-Based Approaches for Fuel Cell Hybrid Electric Vehicles. *Appl. Sci.* **2021**, *11*, 3849. [CrossRef]
8. Lee, J.; Lee, H. A New HEV Power Distribution Algorithm Using Nonlinear Programming. *Appl. Sci.* **2022**, *12*, 12724. [CrossRef]
9. Chen, Z.; Liu, Y.; Zhang, Y.; Lei, Z.; Chen, Z.; Li, G. A neural network-based ECMS for optimized energy management of plug-in hybrid electric vehicles. *Energy* **2022**, *243*, 122727. [CrossRef]
10. Rezaei, A.; Burl, J.B.; Zhou, B.; Rezaei, M. A New Real-Time Optimal Energy Management Strategy for Parallel Hybrid Electric Vehicles. *IEEE Trans. Control Syst. Technol.* **2019**, *27*, 830–837. [CrossRef]
11. Zhang, N.; Ma, X.; Jin, L. Energy management for parallel HEV based on PMP algorithm. In Proceedings of the 2017 2nd International Conference on Robotics and Automation Engineering (ICRAE), Shanghai, China, 29–31 December 2017; pp. 177–182. [CrossRef]
12. Schmid, R.; Buerger, J.; Bajcinca, N. Energy Management Strategy for Plug-in-Hybrid Electric Vehicles Based on Predictive PMP. *IEEE Trans. Control Syst. Technol.* **2021**, *29*, 2548–2560. [CrossRef]
13. Sun, X.; Zhou, Y.; Huang, L.; Lian, J. A real-time PMP energy management strategy for fuel cell hybrid buses based on driving segment feature recognition. *Int. J. Hydrogen Energy* **2021**, *46*, 39983–40000. [CrossRef]
14. Rabinowitz, A.; Araghi, F.M.; Gaikwad, T.; Asher, Z.D.; Bradley, T.H. Development and Evaluation of Velocity Predictive Optimal Energy Management Strategies in Intelligent and Connected Hybrid Electric Vehicles. *Energy* **2021**, *14*, 5713. [CrossRef]

15. Li, X.; Wang, W.; Yuan, Y.; Li, H.; Guo, L.; Qiu, S. An online optimal energy management strategy for a dual-mode power-split hybrid electric vehicle based on hybrid MPC Algorithm. *J. Phys. Conf. Ser.* **2021**, *1754*, 12135. [CrossRef]
16. He, H.; Wang, Y.; Han, R.; Han, M.; Bai, Y.; Liu, Q. An improved MPC-based energy management strategy for hybrid vehicles using V2V and V2I communications. *Energy* **2021**, *225*, 120273. [CrossRef]
17. Hong, J.; Wang, Z.; Chen, W.; Wang, L.; Lin, P.; Qu, C. Online accurate state of health estimation for battery systems on real-world electric vehicles with variable driving conditions considered. *J. Clean. Prod.* **2021**, *294*, 125814. [CrossRef]
18. Xie, S.; Hu, X.; Liu, T.; Qi, S.; Lang, K.; Li, H. Predictive vehicle-following power management for plug-in hybrid electric vehicles. *Energy* **2019**, *166*, 701–714. [CrossRef]
19. de Souza, E.A.G.; Nagano, M.S.; Rolim, G.A. Dynamic Programming algorithms and their applications in machine scheduling: A review. *Expert Syst. Appl.* **2022**, *190*, 116180. [CrossRef]
20. Bellman, R.; Lee, E. History and development of dynamic programming. *IEEE Control Syst. Mag.* **1984**, *4*, 24–28. [CrossRef]
21. Li, D.; Wang, Q.; Wang, J.; Yao, Y.R. Mitigation of Curse of Dimensionality in Dynamic Programming. *IFAC Proc. Vol.* **2008**, *41*, 7778–7783. [CrossRef]
22. Harselaar, W.M.W.; Schreuders, N.; Hofman, T.; Rinderknecht, S. Improved implementation of dynamic programming on the example of hybrid electric vehicle control. *IFAC-PapersOnLine* **2019**, *52*, 147–152. [CrossRef]
23. Ye, Z.; Li, K.; Stapelbroek, M.; Savelsberg, R.; Gunther, M.; Pischinger, S. Variable Step-Size Discrete Dynamic Programming for Vehicle Speed Trajectory Optimization. *IEEE Trans. Intell. Transp. Syst.* **2019**, *20*, 476–484. [CrossRef]
24. Dong, H.; Yin, G.; Zhuang, W.; Chen, H.; Zhou, Y.; Wang, Y. Economic Cruising Velocity Optimization Using Iterative Dynamic Programming of Connected Electric Vehicle. *Ji Xie Gong Cheng Xue Bao* **2021**, *57*, 121. [CrossRef]
25. Bazzi, A.; Berthet, A.O.; Campolo, C.; Masini, B.M.; Molinaro, A.; Zanella, A. On the Design of Sidelink for Cellular V2X: A Literature Review and Outlook for Future. *Access* **2021**, *9*, 97953–97980. [CrossRef]
26. Saboohi, Y.; Farzaneh, H. Model for developing an eco-driving strategy of a passenger vehicle based on the least fuel consumption. *Appl. Energy* **2009**, *86*, 1925–1932. [CrossRef]
27. Shen, P.; Zhao, Z.; Guo, Q.; Zhou, P. Development of Economic Velocity Planning Algorithm for Plug-in Hybrid Electric Vehicle. *IEEE Trans. Intell. Transp. Syst.* **2022**, *23*, 5501–5513. [CrossRef]
28. Yang, H.; Almutairi, F.; Rakha, H. Eco-Driving at Signalized Intersections: A Multiple Signal Optimization Approach. *IEEE Trans. Intell. Transp. Syst.* **2021**, *22*, 2943–2955. [CrossRef]
29. Xu, Y.; Li, H.; Liu, H.; Rodgers, M.O.; Guensler, R.L. Eco-driving for transit: An effective strategy to conserve fuel and emissions. *Appl. Energy* **2017**, *194*, 784–797. [CrossRef]
30. Xiao, M.; Zhao, Z. Economic Velocity Planning and Gear Decision of Plug-In Hybrid Electric Car Passing through the Bend. SAE Technical Paper; SAE International: Warrendale, PA, USA, 2022. [CrossRef]
31. Lin, X.; Wu, J.; Wei, Y. An ensemble learning velocity prediction-based energy management strategy for a plug-in hybrid electric vehicle considering driving pattern adaptive reference SOC. *Energy* **2021**, *234*, 121308. [CrossRef]
32. Chen, Z.; Wu, S.; Shen, S.; Liu, Y.; Guo, F.; Zhang, Y. Co-optimization of velocity planning and energy management for autonomous plug-in hybrid electric vehicles in urban driving scenarios. *Energy* **2023**, *263*, 126060. [CrossRef]
33. Ju, F.; Zhuang, W.-C.; Wang, L.-M.; Liu, J.-X.; Wang, Q. Velocity planning strategy for economic cruise of hybrid electric vehicles. *Zhejiang Da Xue Xue Bao. Gong Xue Ban* **2021**, *55*, 1538.